diversity

MDPI

Article

First Known Cranium of *Cuvieronius* (Proboscidea: Gomphotheriidae) from North America

Peter Houde [1,*], Spencer G. Lucas [2], Matthew Heizler [3], Julia Ricci [3], William J. Boecklen [1] and Brian Hampton [4]

[1] Department of Biology, New Mexico State University, Las Cruces, NM 88003, USA; phoude@nmsu.edu (P.H.); wboeckle@nmsu.edu (W.J.B.)
[2] New Mexico Museum of Natural History and Science, Albuquerque, NM 87104, USA; spencer.lucas@dca.nm.gov
[3] New Mexico Bureau of Geology and Mineral Resources, New Mexico Institute of Mining and Technology, Socorro, NM 87801, USA; matt.heizler@nmt.edu (M.H.); julia.ricci@nmt.edu (J.R.)
[4] Department of Geological Sciences, New Mexico State University, Las Cruces, NM 88003, USA; bhampton@nmsu.edu
* Correspondence: phoude@nmsu.edu

Abstract

We describe the first known complete cranium of an adult *Cuvieronius* from North America, dated to approximately 1.2 Ma, Early Irvingtonian North American Land Mammal Age. It differs in some details from better-known later Andean populations of *Cuvieronius* that may reflect polymorphism, sexual dimorphism, ontogeny, genetic divergence, or erroneously reconstructed specimens. We argue that North/Central American and South American *Cuvieronius* are most logically two genetically distinct cryptic species based on differences in their ages and our inferences about genetic divergence arising from an initial founder effect and/or isolation by distance, followed by allopatry over a long geologic time interval.

Keywords: Gomphotheriidae; *Cuvieronius*; *tropicus*; *hyodon*; GABI; cryptic species; sanidine; radiometric dating; Tshirege eruption; Jemez Volcanic Field; stable isotope

1. Introduction

In the Mesilla basin of Doña Ana County, New Mexico, fossil mammals of Blancan and Irvingtonian age are known from the Camp Rice Formation, strata of the Ancestral Rio Grande and its tributaries [1–4]. In addition to mammalian biochronology, some magnetostratigraphy and radioisotopic age on pumice provide additional age control on the Camp Rice Formation [5,6] Pleistocene proboscideans known from the Mesilla basin include the gomphotheriids *Cuvieronius* (sensu Lucas [7]) and *Stegomastodon*, as well as *Mammuthus* and *Mammut*.

By virtue of the extensive pneumatic sinuses within the delicate neurocranium of proboscideans, skulls of extinct species typically disintegrate once they've reached subaerial erosion horizons. Thus, they are rarely recovered intact except when spontaneously exposed and excavated. We report one such deeply buried, jawless cranium of *Cuvieronius* (Proboscidea: Gomphotheriidae) from the early Pleistocene of the Camp Rice Formation that was discovered during gravel quarrying operations near Bishop Cap, south of Las Cruces, in the Mesilla Basin of the valley of the lower Ancestral Rio Grande (Figure 1). It is the most completely preserved cranium of the genus yet discovered in North America, and among the few well-preserved examples yet known throughout its paleogeographic range in the Americas.

Check for updates

Academic Editor: Michael Wink

Received: 30 December 2025
Revised: 25 January 2026
Accepted: 26 January 2026
Published: 3 February 2026

Copyright: © 2026 by the authors. Licensee MDPI, Basel, Switzerland. This article is an open access article distributed under the terms and conditions of the Creative Commons Attribution (CC BY) license.

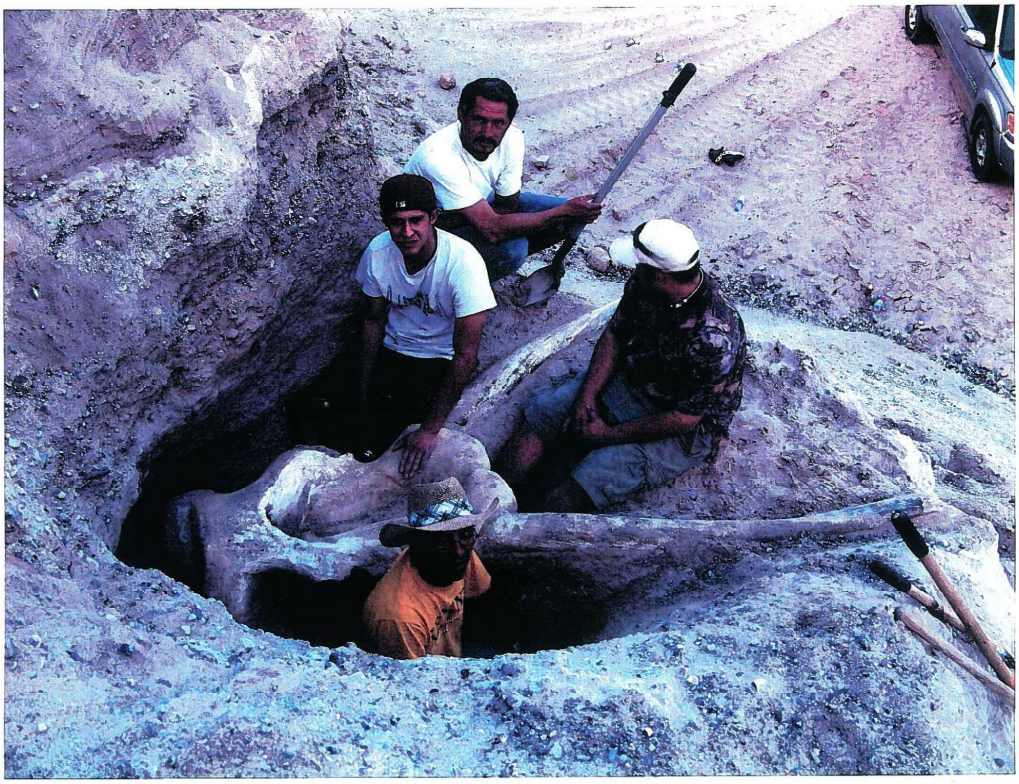


Figure 1. *Cuvieronius* cf. *tropicus* NMSU 15722, as found and excavated prior to 2010 by quarry workers near Mesquite, New Mexico, showing the pristine condition of the nuchal and supraorbital regions prior to subsequent damage caused by repeated excavation and reburial. Over the course of years, the specimen was undermined without support or application of preservative. It is not clear whether the nasal process was ever preserved, as there are no photos in which it was present, and no vestige of it was found.

Quite a bit is known of the cranial morphology of *Cuvieronius* from a population of at least dozens of individuals from the late Pleistocene in Tarija, Bolivia. It includes a broad representation of age classes and presumably both sexes [8,9]. The Tarija specimens are considerably disparate geographically and chronologically. We argue herein that they would almost certainly be recognized as sufficiently distinct genetically to be considered a distinct, South American species of *Cuvieronius*, if such data were available. Hence, we resurrect the North American species *C. tropicus* and tentatively refer the new specimen to it.

The new material permits new comparisons and perspectives on some features of *Cuvieronius*. It also permits a new comparison to the nearly coeval and geographically proximate *Rhynchotherium* (sensu [10]), an exceptionally complete skull of which (LVMNH 871) is known from the slightly older Pliocene Gila Conglomerate, near Sheldon, Greenlee County, Arizona, within 5 km of the New Mexico border [11].

2. Methods

2.1. Institutional Abbreviations

LVMNH, Las Vegas Museum of Natural History; MNPA, Museo Nacional de Paleontología y Arqueología, Tarija, Bolivia; MACN, Museo Argentino de Ciencias Naturales 'Bernardino Rivadavia', Buenos Aires, Argentina; MNHN, Muséum national d'Histoire naturelle in Paris, France; MUSM-Ncn, Museo de Historia Natural, Instituto Geologico Minero y Metalúrgico, Lima, Peru; NMSU, New Mexico State University Vertebrate Museum, Las Cruces, USA.

2.2. Comparative Material Examined

Cuvieronius hyodon (NMHN TAR 1270), *Rhynchotherium* cf. *falconeri* (LVNHM 871), *Stegomastodon mirificus* (NMSU 15723), *Mammut americanum*, *Mammuthus columbi*, *Mammuthus primigenius*, *Loxodonta africana* (uncatalogued).

2.3. Anatomical Terminology

Terminology follows van der Merwe et al. [12], except as noted.

2.4. Conservation

NMSU 15722 was originally found with no detectable damage or diagenetic distortion other than the absence of the nasal process (Figure 1). It suffered both superficial and structural damage over the course of several years of repeated unearthing and reburial by quarry workers (Figures 1 and S1). It was ultimately recovered in pieces and reassembled. Polyvinyl butyrate was used as a hardener and preservative. In the laboratory, bone fragments were fully immersed in a solution of polyvinyl butyrate in acetone for several days and then allowed to fully dry before any reassembly was attempted. No two pieces were joined together unless they contacted unambiguously, and matched in color and morphology internally, externally, and in section. Fiberglass and Cab-O-Sil (Cabot Corporation, Boston, MA, USA) amorphous silica microspheres in polyester resin were used to fill or reconstruct missing fragments, notably the supraorbital region and postorbital processes of the frontal bones and lateral parts of the nuchal region, guided with the aid of multiple photographs taken of the specimen in situ before it was damaged.

2.5. $^{40}Ar/^{39}Ar$ Age Determination

Detrital sanidine (DS) was concentrated by standard methods from sample BQM-CR-01 (the site of NMSU 15722 excavation) and dated by the $^{40}Ar/^{39}Ar$ method. Detailed analytical data are provided in Supplement S2 and briefly described here. The sample was irradiated at the USGS reactor in Denver, Colorado for 7 h. The Fish Canyon tuff standard, with an age of 28.201 ± 0.023 Ma [13], was used as a flux monitor. Crystals were fused using a CO_2 laser, and extracted argon isotopes were measured using an ARGUS VI multi-collector mass spectrometer (Breman, Germany). The maximum depositional age was calculated based on the inverse variance weighted mean of the youngest normally distributed population of dates based on the mean square of weighted deviations (MSWD). Age calculation used a total decay constant for ^{40}K of 5.463×10^{-10}/a [13]. Age uncertainty is reported at ±1σ and includes the error of the J-factor and neutron interferences.

2.6. Stable Isotope Analysis

We prepared a small sample of enamel from the spiral band of the tusk following protocols outlined in [14,15]. After surface cleaning, dentine and cementum were removed with a diamond bit rotary tool. Powdered enamel was soaked in 30% H_2O_2 for 24 h to remove sedimentary carbonates and residual organic matter. The sample was then rinsed five times with purified water, filtered, and dried. Twice, the sample was soaked in 0.1 M acetic acid for three days, rinsed five times with purified water, and dried.

All isotopic analyses of samples were performed in the Laboratory for Environmental Chemistry at New Mexico State University. Samples were combusted using a Costech Analytical Elemental Analyzer (Model ESC 4010, Valencia, CA, USA) and introduced to a ThermoFinnigan DeltaPlus XP Isotopic Ratio Mass Spectrometer (Bremen, Germany) in continuous flow through a ConFlo III Interface. Results are described in delta (δ) notation in measures of "per mil" (‰), or per parts per thousand. Results are reported as the difference between the isotopic ratio of the sample and the international standard, "VPDB"

(Vienna Pee Dee Belemnite, a carbonate rock), for ^{13}C. Values are standardized using the following formula:

$$\delta^{13}C = [(R_{sample} - R_{standard})/R_{standard}] \times 1000$$

where $R = {}^{13}C/{}^{12}C$. All analyses are traceable to the NIST (National Institute of Standards and Technology, Washington, DC, USA) isotopic standard reference materials USGS24 and NBS-19.

3. Systematic Paleontology

Order Proboscidea Illiger, 1811 [16].
Family Gomphotheriidae Hay, 1922 [17].
Genus *Cuvieronius* Osborn, 1923 [18].
Cuvieronius cf. *tropicus* (Cope, 1884) [19].

3.1. Referred Specimen

NMSU 15722 is a fully adult cranium, preserving bilaterally I1, M2 (all lophs fully worn), M3 (mesial two lophs worn), but lacking the mandible, right zygomatic, nasal process, supraorbital regions and postorbital processes (=zygomatic process of the frontal per [12]) bilaterally, dorsolateral nuchal regions bilaterally, pterygoid hamuli bilaterally, and approximately 20% of distal end of the left I1.

3.2. Locality

It was collected in a privately owned gravel quarry northeast of the unincorporated community of Mesquite and on the west flank of Bishop Cap, Mesilla Valley, Doña Ana County, New Mexico, T24S R3E section 28 San Miguel Quadrangle, 32°1′35.7612″ N 106°38′26.6604″ W (32.193267, −106.640739), elevation 1268 m. Locality 9860, New Mexico Museum of Natural History and Science, Geoscience collection database.

3.3. Geological Context: The Camp Rice Formation

The Camp Rice Formation records axial–fluvial and alluvial fan sedimentation that took place in the Mesilla basin in southernmost Central New Mexico (as well as in the more southerly Hueco basin of West Texas and northernmost Mexico) during the Plio–Pleistocene [20,21]. In the Mesilla basin, the Camp Rice Formation is mapped as two distinct facies that represent axial–fluvial sedimentation of the Ancient Rio Grande, and a piedmont slope facies (alluvial fan sedimentation) located along the slopes of regional highs along the margins of the basin [22]. All vertebrate fossil localities occur in channelized axial–fluvial strata that consist of very weakly indurated, medium- to coarse-grained, cross-stratified sandstone and isolated pebble conglomerate, as well as fine-grained floodplain strata consisting of laminated mudstones with interbedded very fine-grained sandstone [21,23]. The overall thickness of the Camp Rice Formation varies throughout the Mesilla basin, ranging from 40 to 135 m, with some of the thickest strata occurring along the western margin of the basin [6].

Biostratigraphic age constraints for the Camp Rice Formation consist of several Blancan–Irvington fossil localities that include occurrences of *Stegomastodon mirificus*, *Mammuthus columbi*, and *Tapirus* [24–26]. Numerical ages are best constrained by four distinct, granule- to pebble-size pumice beds that have been dated at 1.3, 1.6, 2.0, and 3.1 Ma. The two most widespread pumice layers are the 1.6 Ma pumice that correlates with the Otowi Member of the Bandelier Tuff and the 3.1 Ma pumice layer that correlates with the Grants Ridge rhyolite complex [6,27,28]. Several tephra layers are also interbedded in Camp Rice strata and include the 1.59–1.22 Ma Las Palomas Ash and the 2 Ma Huckleberry Ridge

Ash [6]. Magnetostratigraphy was applied to the Camp Rice Formation across Southern New Mexico. Basal strata overlap with the Gauss geopolarity chron and Mammoth and Kaena subchrons. The uppermost strata span the Matuyama–Brunhes chron, suggesting that the age of the Camp Rice Formation spans from 3.6 to ~0.80 Ma [23] (Figure 2).

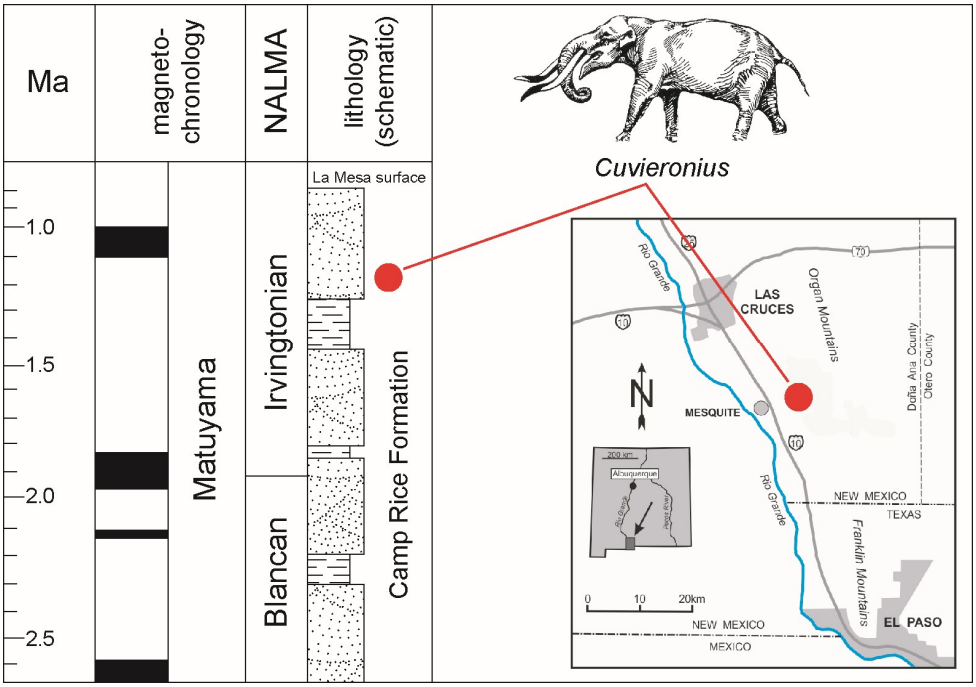


Figure 2. Location of the *Cuvieronius* skull NMSU 15722 near Bishop Cap, southeast of Las Cruces, New Mexico, and stratigraphic position of the fossil in a schematic lithologic column of the Camp Rice Formation. Numerical ages (Ma, millions of years), magnetochronology, and North American Land Mammal Age (NALMA) based on [5].

3.4. Geologic Horizon

For the Camp Rice Formation of the Santa Fe Group, $^{40}Ar/^{39}Ar$ detrital sanidine radioisotopic dating yields a maximum depositional age (MDA) of early Irvingtonian North American Land Mammal Age (NALMA) age at 1.252 ± 0.003 Ma (1σ), or possibly as young as 1.2319 ± 0.001 Ma (2σ), if sanidine is directly derived from the Tshirege eruption of the Jemez Volcanic Field, New Mexico (Section 7, below). Less precisely, the site maps geographically within the Matuyama Chron are dated by a reversed magnetostratigraphy, radioisotopically and tephrochronologically dated volcanic rocks, and vertebrate biostratigraphy to 2.6 to 0.78 Ma [6]. Stratigraphically, it is ~15 m below a 1.6 Ma pumice bed and ~24 m below the La Mesa surface, which is considered to be about 0.8 Ma (Figure 2). This suggests alternatively that the skull could be late Blancan NMLMA, approximately coeval with Vanderhill's [2] Mesilla basin Fauna B (renamed the La Union Fauna [4]), which also yields dental material assigned to *Cuvieronius*. Nevertheless, we suggest that our new 1.2 Ma MDA is the most accurate age of the *Cuvieronius* skull, so we regard it as of early Irvingtonian age.

3.5. Taphonomic Setting

NMSU 15722 was preserved in coarse-grained alluvium, representing fluvial channel sediment of the axial portion of the lower Ancient Rio Grande in the central Mesilla Basin. Mack et al. [6] describe the Ancient Rio Grande as "a braided stream floored by channel bars and trains of three-dimensional dunes that transported pebbly medium to coarse sand. Axial-fluvial sediment is locally interbedded with alluvial-fan conglomerates and

gravelly sandstones." Vertebrate fossils from the Camp Rice Formation are almost always isolated bones, isolated tusks, teeth or dentaries, and occasionally skulls that have been disarticulated and transported to some extent. The surface texture of NMSU 15722 shows no indication of subaerial weathering and no overt evidence of activities by scavengers before burial. The absence of any associated disarticulated elements, including the mandible, suggests that the skull might have become entrained in the Ancestral Rio Grande and transported very little if at all downstream before stranding in its most stable horizontally level orientation, dorsal side up. It likely represents a gomphothere that lived near the river and died there. Other postcranial fossils and a proboscidean dentary not available for our examination had been found in the quarry previously, but reportedly none in proximity to NMSU 15722.

3.6. Differential Diagnosis of NMSU 15722

Trilophodont molars with well-developed postrite central conules and trefoils, and tusks with a spiral band of enamel, distinguish *Cuvieronius* from all other Gomphotheriinae except *Rhynchotherium*. The latter is most readily distinguished from adult specimens of *Cuvieronius* by the presence of i1 [29], but NMSU 15722 lacks the mandible. Nevertheless, NMSU 15722 is distinguished from *Rhynchotherium* by its low dorsal profile of the cranium with a flattened frontoparietal region or 'forehead'; a cranium that is not "domed" in lateral profile as in *Rhynchotherium* (Figure S2); and a substantially younger geological horizon. *C. tropicus* is recognized herein as a North and Central American species, distinct from *C. hyodon* from South America, based on presumed genetic differentiation that we infer from biogeographic models of gene flow and speciation (Section 9.4, below).

4. Description

4.1. Dorsal Aspect

The cranium is at its widest as measured bilaterally across the nuchal crest and temporal bones, next across the postorbital processes of the frontals, and then across the premaxillae (=incisive [12]) and maxillae. It is markedly narrow between the temporal lines across the frontal and parietal bones, more so than the width of the external nares, as defined by the right and left margins of the supraorbital ridge (Figure 3, Table 1). The minimum distance between the base of the tusks is less than the minimum bilateral width of the maxillae. The rostral-most margins of the premaxillae between the tusk alveoli are straight and blunt rather than rounded, and slightly longer (rostrally) laterally than medially. Lateral to this, the rostral margin of the premaxillae, i.e., the tusk alveolar margin, is sharply angled laterally 110° to 120°. At their rostral end, the gap between the right and left premaxillae is uniformly narrow. The sutures of the neurocranium are mostly fully fused and obliterated or nearly so (Figure 4), whereas the premaxillary–maxillary sutures are unfused. The caudal-most portion of the maxillae is visible dorsally, where they extend as broad and medially convex lappets on the lateral surface of the premaxillae. The infraorbital foramen is located in the malar notch and faces rostrolaterally. The dorsal surface of the neurocranium is considerably shorter rostrocaudally (measured caudally from the nasal cavity because the nasal process is damaged) than it is in width between the temporal fossae. The lateral portion of the nuchal crest is deflected caudally beyond the dorsal/medial portion (Figure 1), but this region was irreparably damaged prior to specimen collection and, therefore, cannot be thoroughly described.

The single, large external nares is located just caudal to the visible symphysis of the premaxillae. The "incisive fossa" (sensu [30], i.e., the dorsomedial surfaces of the palatine processes of the premaxillae, not equivalent to the same term formally used in association with the nasopalatine nerve and greater palatine vessels) is wide and shallow rostrally,

but deep, narrow, and well-defined caudally, medial to the supraorbital ridges. Thus, the overall shape of the incisive fossa is teardrop-like, with the point directed caudally, less ovoid and less well-defined rostrally than in *Loxodonta*. The fossa terminates caudally as small bilateral pits, which we refer to as infranasal fossae, that are separated from the external nares by a low crest. Lateral to this, the rostral margin of the external nares is poorly defined by a low ridge and slopes more gradually onto the premaxillae, more like *Rhynchotherium* (Figure S3) than *Mammut*, *Mammuthus*, and *Loxodonta*.

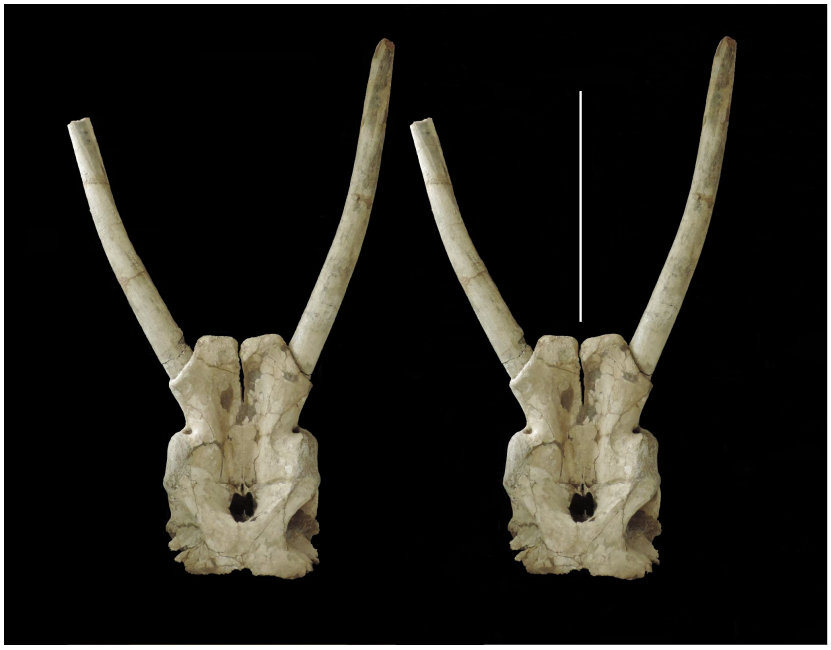


Figure 3. *Cuvieronius* cf. *tropicus* NMSU 15722, dorsal stereophotograph, photographed from 6 m distance and with tusks oriented (dorsoventrally) vertically to mitigate parallax. Scale bar 1 m.

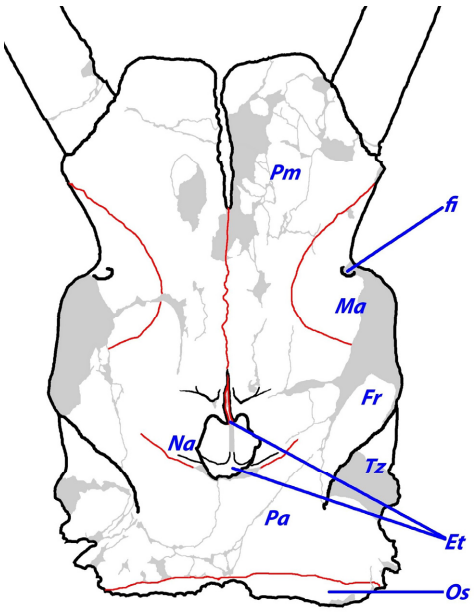


Figure 4. *Cuvieronius* cf. *tropicus* NMSU 15722, dorsal view, labeled line drawing. Shading indicates surface damage or regions reconstructed based on photographs of the specimen as it was first discovered. Red lines indicate visible sutures. Abbreviations: Et—ethmoid; fi—infraorbital foramen; Fr—frontal; Ma—maxilla; Na—nasal; Os—supraoccipital; Pa—parietal; Pm—premaxilla (=incisive [12]); Tz—temporal, zygomatic process.

Table 1. Measurements (in mm).

Dorsal length (premaxillae to occiput)	940
Preorbital length *	480
Postorbital length *	450
Maximum bilateral width (alveolar processes) of premaxillae	380
Width between infraorbital foramina	450
Width across orbits *	650
Minimum bilateral width between temporal lines	350
Minimum width occiput *	710
Maximum width incisive fossa	490
Width external nares	120
Depth incisive fossa	10
Bizygomatic width of temporals	700
Width occipital condyles	200
Diameter of foramen magnum	73
Maximum width of palate	300
Maximum width internal nares	60
Maximum length internal nares	130
Width of mandibular facies	165
Length of premaxillae rostral to M2	400
Depth tooth row alveoli to skull roof above orbit	520
Depth mastoid to skull roof	400
Diameter orbit *	130
Height occipital crest to top of foramen magnum	450
Width nuchal fossa	105
Tusk length (R)	>1500
Diameter of base of tusk min × max (R)	134 × 137
Diameter of base of tusk min × max (L)	132 × 141
Circumference of base of tusk (R)	432
Circumference of base of tusk (L)	435
Maximum width of enamel band (R)	60
Maximum width of enamel band (L)	58
M2 length × width	140 × 90
M3 length × width	174 × 92

* estimated.

The tusks are nearly straight but very slightly convex laterally, such that they are continuously divergent and not parallel throughout their lengths. The enamel band completes less than one revolution around the tusk, is relatively narrow, and attenuates to the point of nonexistence for the proximal 50–58% of the nonalveolar portion of the tusk. The tusks exhibit no evidence of use-wear. The tusks are rooted in alveoli that form an angle of about 55° from one another, as measured from where their axes converge or 26–27° from the parasagittal plane, measured from the longitudinal level of the malar notch with the long axis of the skull.

4.2. Ventral Aspect

The basioccipital portion of the skull caudal to the internal nares is half the length of the premaxillary portion and palate rostral to the internal nares (Figure 5). At the rostral end, the sutures between the premaxillae (dorsally) and the palatine ledge of the maxillae (ventrally) are unfused. At their rostral-most margins, the inferior rims of the premaxillae and the rims of the maxillae are slightly convex, thickened, and slightly rugose. The premaxillae wrap around the ventral aspect of the tusk base to form a thin flange of bone around the ventral alveolar margin at the tusk base.

M2 aligns with the malar notch. M3 extends caudally nearly half the length of the masseteric fossa or infratemporal fossa, defined as medial to the zygomatic arch. The molar

rows diverge slightly rostrally. A small greater palatine foramen lies close and medial to the fourth loph of M3 within the palatine bone. The masseteric fossa is subround, being slightly longer than wide. Its caudal margin is formed by the mandibular facies, which is twice as wide as long and mediolaterally concave. The ventral aspect of the skull is at its narrowest, measured across the pterygoid processes of the sphenoid. The condylar fossa caudal to the mandibular facies is a shallow sulcus that narrows laterally to a point, i.e., the tympanic incisure. The foramen rotundum lies directly rostral to the foramen ovale, immediately medial to the mandibular facies of the temporal bone. The small pharyngotympanic canal lies medial to them, forming an equilateral triangle. The jugular foramina are immediately rostral to the occipital condyles. The occipital condyles form the caudal-most part of the skull, are longer than wide, and converge somewhat rostrally.



Figure 5. *Cuvieronius* cf. *tropicus* NMSU 15722, ventral stereophotograph, photographed from 6 m distance and with tusks oriented (dorsoventrally) vertically to mitigate parallax.

The internal nares is attenuated rostrally, longer than wide, and about one-third the bilateral width of the pterygoids and sphenoid bones lateral to it. The basioccipital is long and narrow, especially rostrally. The petrosal portion of the temporal bone is relatively small. It is more or less circumscribed by five foramina: rostrally by the pharyngotympanic canal, medially by the carotid canal within it, caudally by the jugular foramen that interrupts the temporal–occipital suture immediately rostral to the occipital condyle, laterally by the stylomastoid foramen within the medial retrotympanic process of the temporal (or possibly exoccipital) bone, and the foramen ovale rostrolaterally within the caudal-most extension of the sphenoid (Figure 6). The pharyngotympanic canal is minute, and the carotid canal, stylomastoid foramen, and jugular foramen are intermediate in size between it and the foramen ovale. Lateral to the condyles, the exoccipital extends laterally to a parasagittally straight suture with the retrotympanic process of the temporal.

4.3. Lateral Aspect

The skull is about 75% of the length of the complete right erupted tusk and is low vaulted. The dorsal surface of the neurocranium, formed by the frontal and parietal bones,

is slightly concave rostral to the nuchal crest. Furthermore, the supraorbital region of NMSU 15722 lies within or below the plane defined by the dorsal-most points of the premaxilla and the nuchal crest, lending a somewhat dish-faced appearance (Figures 7 and 8). The angle of the "face", as measured from the plane of the highest points of the rostral premaxillae to the occipital relative to the plane of the occlusal surface of the molars, is shallow (Table 2).

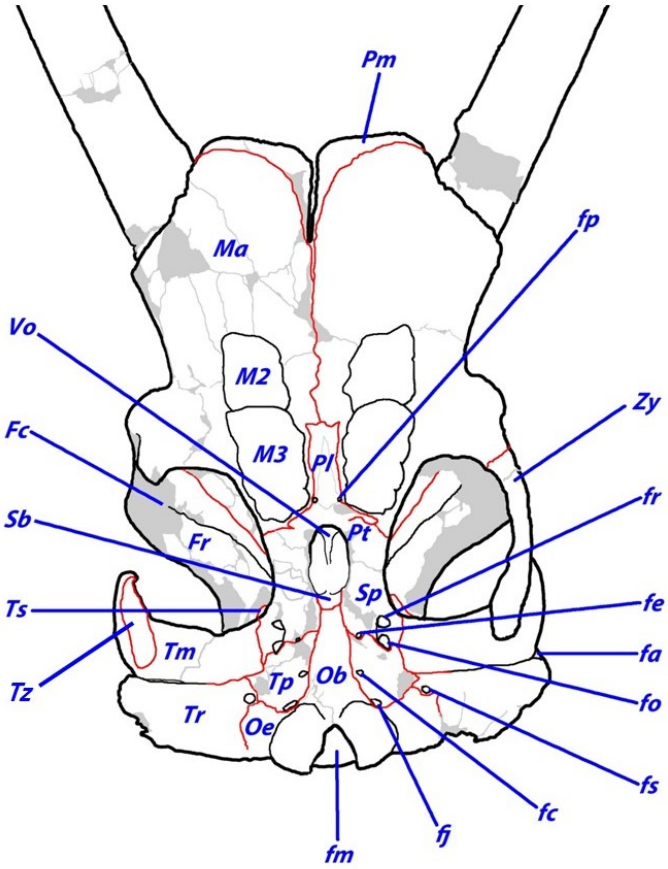


Figure 6. *Cuvieronius* cf. *tropicus* NMSU 15722, ventral view, labeled line drawing. Shading indicates surface damage or regions reconstructed based on photographs of the specimen, as it was first discovered. Red lines indicate visible sutures. Abbreviations: fc—carotid canal; Fc—orbitotemporal crest; fe—pharyngotympanic canal; fj—jugular foramen; fm—foramen magnum; fo—foramen ovale; fp—greater palatine foramen; fr—foramen rotundum; Fr—frontal; fs—stylomastoid foramen; Ma—maxilla; Ob—basioccipital; Oe—exoccipital; Pl—palatine; Pm—premaxilla (=incisive [12]); Pt—pterygoid; Sb—sphenoid (basisphenoid); Sp—sphenoid (pterygoid process); Tm—temporal, mandibular facies; Tp—temporal, petrosal; Tr—tympanic, retrotympanic process; Ts—temporal, squamous portion; Tz—temporal, zygomatic process; Vo—vomer; Zy—zygomatic.

The left maxilla and zygomatic are ankylosed, whereas the right are not, and the right zygomatic bone is missing. The zygomatic arch is nearly uniform in height throughout its length, except caudally, where the zygomatic and temporal articulate. The longitudinal axis of the zygomatic bone is nearly parallel with the occlusal plane of the molars. Its caudal half is thin and forms a loose semicircular articulation with the zygomatic process of the temporal bone. The external auditory meatus is a relatively large, round foramen, located dorsal to the tympanic incisure and midway of the height of the caudal end of the zygomatic process of the temporal bone.

The orbitotemporal crest extends from the orbital fissure to the postorbital process of the frontal bone, thus separating the orbital facies from the temporal fossa (Figure 9). It is oriented diagonally and convex rostroventrally. The temporal line is rounded and poorly

defined. It forms the dorsal margin of the temporal fossa, and it blends with the nuchal crest caudally. The occiput is inclined very slightly caudally from the occipital condyle.



Figure 7. *Cuvieronius* cf. *tropicus* NMSU 15722, right lateral stereophotograph, photographed from 6 m distance and with tusks oriented (dorsoventrally) vertically and bilaterally balanced.



Figure 8. *Cuvieronius* cf. *tropicus* NMSU 15722, left lateral view, photographed from 6 m distance and with tusks oriented (dorsoventrally) vertically and bilaterally balanced.

The tusks have a very slight sinusoidal curvature that is convex dorsally along their proximal half and convex ventrally along their distal half. The rostral-most extent of the premaxillae is thicker, forming a cuff-like dorsolateral margin in comparison to the more caudal sleeve-like portion.

The occlusal surface of the molars is flat, but the alveolar margin is slightly convex or sigmoidal. With the molar occlusal surface oriented horizontally, the longitudinal length of the molars extends from the rostral margin of the orbit to just rostral to the rostral extent of the zygomatic–temporal articulation, more caudad than they appear in the ventral view.

4.4. Caudal Aspect

The extensively pneumatized occiput of NMSU 15722 is the most damaged portion of the skull (Figure 10). As best as can be determined from photographs of the specimen in situ

(Figure S1), the profile was widest at the level of the zygomatic arch and narrowed slightly before widening again dorsolaterally. The profile is considerably more broadly ovoid or rectangular than that of *Loxodonta*. The caudal surface of the nuchal (parietal/occipital) crest is pleated and concave in its medial portion. All sutures of the caudal neurocranium, including the supra- and exoccipitals and the temporal bones, are completely coossified and obliterated. A notch separates the occipital condyles from the exoccipitals ventrally.

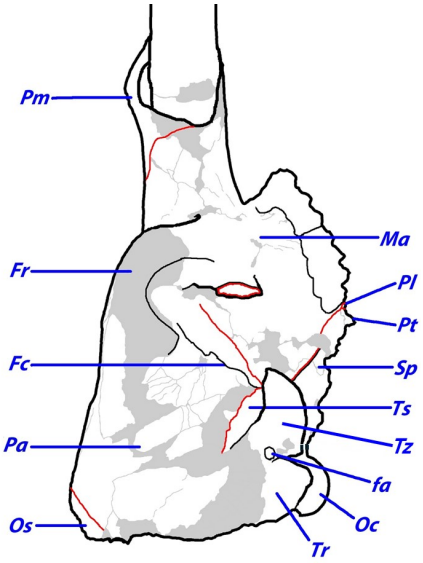


Figure 9. *Cuvieronius* cf. *tropicus* NMSU 15722, right lateral view, labeled line drawing. Shading indicates surface damage or regions reconstructed to the extent possible based on photographs of the specimen as it was first discovered. Red lines indicate visible sutures. Abbreviations: fa—external auditory meatus; Fc—orbitotemporal crest; Fr—frontal; Ma—maxilla; Oc—occipital condyle; Os—supraoccipital; Pa—parietal; Pl — palatine; Pm—premaxilla (=incisive [12]); Pt—pterygoid; Sp—sphenoid (pterygoid process); Tr—tympanic, retrotympanic process; Ts—temporal, squamous portion; Tz—temporal, zygomatic process.

Table 2. Comparative angle measurements in lateral view (in degrees).

Angle	*C.* cf. *tropicus* [1]	*C. hyodon* [2]	*Rhynchotherium* [3]	*Loxodonta* [4,5]	*Elephas* [5]
A	28 (R), 31 (L)	27 (R), 31 (L)	31 (R), 44 (L)	81 [4], 62 [5]	83
B	21 (R), ~24 (L)	~21 (R), ~29 (L)	~20 (R), ~31 (L)	~71 [4], 66 [5]	57
C	41 (R), 42 (L)	~34 (R), ~35 (L)	41 (R), ~45 (L)	77 [4], 70 [5]	85
D	~30 (R), ~36 (L)	~30 (R), ~35 (L)	~31 (R), ~36 (L)	70 [4], 73 [5]	59
E	−6 (R), −4 (L)	−4 (R, L)	−3 (R), −4 (L)	161 [4], 153 [5]	165
F	5 (L)	~8 (R), ~6 (L)	9 (R), ~12 (L)	18 [4], 11 [5]	30

Angle Descriptions: A—angle of the occlusal plane of the molars relative to the longitudinal axis of the tusk alveoli; B—angle of the plane of the alveolar margin of the molars relative to the longitudinal axis of the tusk alveoli; C—angle of the "face", as measured from the occlusal plane of the molars relative to the plane defined by the highest points of the rostral premaxillae to the dorsal-most point of the cranium (note: this is the occipital of NMSU 15722, but the non-homologous frontoparietal region of *Rhynchotherium*, *Loxodonta*, and *Elephas* due to their elevated and rounded frontoparietal region, and ignoring the dorsally elevated supraorbital of *Loxodonta* and *Elephas*); D—angle of the "face", as measured from the plane of the alveolar margin of the molars relative to the plane defined by the highest points of the rostral premaxillae to the dorsal-most point of the cranium (note: this is the occipital of NMSU 15722, but the non-homologous frontoparietal region of *Rhynchotherium*, *Loxodonta*, and *Elephas* due to their elevated and rounded fronto-parietal region, and ignoring the dorsally elevated supraorbital regions of *Loxodonta* and *Elephas*); E—elevation of the supraorbital region relative to the planes defined by the highest points of the rostral premaxillae and to the dorsal-most point of the neurocranium, respectively, to it; F—angle of the longitudinal axis of the zygomatic vs. the occlusal plane of the molars; Footnotes: [1]—NMSU 15722; [2]—NMHN TAR 1270 (neotype); [3]—cast of LVMNH 871; [4]—uncatalogued specimen; [5]—unnumbered fig., pp. 56–57 in [31].

The nuchal fossa, successfully reassembled subsequent to photographing Figure 10, occupies half the entire height of the skull from the foramen magnum to the nuchal crest. It is approximately half as wide as it is tall. Its dorsal half is separated by the external occipital crest into a pair of much deeper, very well-defined, heavily pitted depressions. This fossa and the slightly concave lateral portions of the upper occiput are all developed in the supraoccipital, although no sutures are visible in caudal view. The rostral portion of the foramen magnum is narrow, but its caudal margin is rounded and wider than a single occipital condyle. The lateral suture of the exoccipitals to the temporals cannot be determined in caudal view.



Figure 10. *Cuvieronius* cf. *tropicus* NMSU 15722, caudal view stereophotograph, prior to successful reassembly of much of the left lateral occiput and nuchal fossa.

4.5. Molars

The palate bears four cheek teeth, the left and the right M2–3 (Figure 11). The M2s have three lophs and are much more worn than the M3s. Unworn enamel on all of the teeth is ptychodont. On the right M2, a pretrite trefoil is evident between the first and second lophs. Presumably, such trefoils were present between all the M2 lophs, but, because of heavy wear, that cannot be confirmed. There do not appear to be other trefoils, pillars, or tubercles between the lophs, and there is no medial longitudinal sulcus on the crown. Thus, the crowns of the M2s are relatively simple in structure compared to some other taxa, such as *Gomphotherium*. The M2 lophs are nearly perpendicular to the long axis of the tooth. However, wear on loph 1 (protoloph) has resulted in more wear on the labial part of the loph (the pretrite) than on the lingual part of the loph (the posttrite), such that the anterior edges of the M2s are oblique to their long axes.



Figure 11. *Cuvieronius* cf. *tropicus* NMSU 15722, molars stereophotograph.

The M3s bear four lophs and a small, narrow talon posteriorly. Pretrite trefoils are evident, especially on the first two lophs (protoloph and metaloph). No other trefoils, pillars, or tubercles are present in the valleys between the lophs, so the M3s, like the M2s, have a relatively simple crown structure. There is a cingulum at the crown base posteriorly, wrapping around the bases of the fourth loph (tetartoloph) and talon. No median sulcus is present, as the pretrite and postrite portions of the lophs are joined to each other at a "seam."

5. Comparative Description

5.1. Compared with South American Cuvieronius hyodon

The most conspicuous differences between NMSU 15722 and the South American *Cuvieronius*, as illustrated in Boule and Thevenin (Figures 4–9, pls. 1–3 in [9]), Prado and Alberdi (Figures 2C and 3B in [32]; Figure 2 in [33]), and Mothé and dos Santos Avilla (Figure 1B in [30]), are that, in the latter, (1) the right and left external nares are widely separate or "dumbbell shaped" [34]; (2) the medial margins of the premaxillae are widely divergent (Figure 1C, but not 1B, in [30]); (3) in dorsal view, the rostral-most margins of the premaxilla medial to the tusks are angled laterally in line with the alveolar margin, (4) the zygomatic arches are more robust; (5) the tusks are more curved, such that distally they are parallel or nearly so; and (6) the enamel band is broader. Some of these differences in South American specimens are variable. A specimen identified as a juvenile (Figure 3B in [32]) exhibits similar widely separate external nares and divergent premaxillae as those of fully adult specimens, whereas MNPA-V 006194 (Figure 1B in [30]) does not and, so, is inferred to not be related to ontogeny (Figure 3B in [32]). Other specimens illustrated (Figure 1C in [30]) or on display in the Museo Nacional de Paleontología y Arqueología, Tarija, Bolivia [35,36] exhibit premaxillae that are closely spaced and not divergent, like those of NMSU 15722 (Section 6, below).

In lateral view, the presumed male neotype of *C. hyodon* (MNHN TAR 1270, Figure 1 of pl. 1 in [9]) exhibits a profoundly more massive zygomatic arch that is thicker and taller at the level of the external auditory meatus, such that the ventral margin of the zygomatic process of the temporal is disproportionately deeper from the meatus than the dorsal margin, is more extensive caudally, and its dorsal surface continues caudally at a low angle to join the nuchal crest uninterrupted to enclose a very well-defined temporal fossa. However, it is unclear just how many of these features are reconstructed in MNHN TAR 1270 (Figure S4). NMSU 15722 possesses a much more gracile zygomatic arch, the longitudinal axis of which is approximately in line with the external auditory meatus. The poorly defined but heavily damaged lateral portion of the nuchal crest rises from the zygomatic arch at what appears to be closer to a right angle than in MNHN TAR 1270. The orbit of MNHN TAR 1270 appears to be much smaller relative to the cranium overall than that of NMSU 15722. However, both the ventrally projecting postorbital process of the frontal and the dorsally projecting postorbital process at the maxillary–zygomatic suture that define the orbit of MNHN TAR 1270 appear to be reconstructed (Figure S4). The frontal bones of NMSU 15722 are also partly reconstructed, and the intact left zygomatic arch of NMSU 15722 exhibits only the barest indication of the caudal extent of the orbit.

In further comparison to the neotype of *C. hyodon* (MNHN TAR 1270, [7]; Figures 4–9, pls. 1–3 in [9]), the tusks of NMSU 15722 are straighter and widely divergent, and the premaxillae between the tusk alveoli are robust and pronounced rostrally. Their combined rostral-most margin forms a nearly straight line medial to the right and left tusks in the dorsal or ventral views. Lateral to this, the alveolar margin of the maxillae forms a marked angle (left 120°, right 112°), as viewed from above, such that the lateral alveolar margin is much reduced in NMSU 15722. This is quite different from MNHN TAR 1270, in which the

rostral margins of each of the right and left premaxilla and maxilla, i.e., the rostral margin of the alveoli and the area medial to it, are inferred to form a straight line, facing somewhat caudolaterally, but note that this region of the skull is reconstructed (Figure S4).

The incisure between the right and left premaxillae of NMSU 15722 is narrow and long, whereas this is inferred to have been wide and short by Boule and Thevenin (Figure 5 in [9]), despite the fact that the tusk alveoli of NMSU 15722 are equally divergent (NMSU 15722, 50°; Tarija specimen, 48°, measured from Figure 1 of pl. 2 in [9]). Prado and Alberdi (Figure 2 in [33]) highlighted this region of the skull as "the most important" difference distinguishing the skull of *Cuvieronius* from that of *Notiomastodon* (referred to as *Stegomastodon* by [32,33]) [37]. The tusks of NMSU 15722 are straighter and, therefore, significantly more widely divergent distally than in MNHN TAR 1270, which curve medially and are nearly parallel to one another for much of their length. Boule and Thevenin [9] state that the left tusk of their specimen could be faithfully rejoined to the root ("Its proximal portion, or the root, having remained in the alveolus, the rest has been precisely replaced, thanks to the net shape of the break") and that it was intact for the rest of its length. The right tusk was reconstructed as a mirror image of the left. The difference in tusk divergence could result from more pronounced torsion of the tusks in MNHN TAR 1270, which Boule and Thevenin [9] hypothesized was a sexually dimorphic character. The tusks of some other *Cuvieronius* from Tarija exhibit even more pronounced sigmoidal curvature than MNHN TAR 1270 [38].

Boule and Thevenin described and illustrated (Figures 1 and 2 of pl. 3 in [9]) "pronounced and clearly visible" crests/ridges extending rostrally from the molars on the ventral surface of the maxillae in both juvenile and adult Tarija specimens. The ridges are clearly evident throughout the length of the maxillae (Figure 2 of pl. 3 in [9]) and in a specimen identified as female by Nordenskiöld (Figure 2 of pl. 1 in [8]), but only in the caudal portion of the maxillae in MNHN TAR 1270 (Figure 1 of pl. 3 in [9]). These ridges are inconspicuously present and uniformly divergent rostrally in NMSU 15722. In the caudal view, the contour of the occiput of NMSU 15722 is much more rounded than the bilaterally broad, nearly rectangular profile of the specimen illustrated by Boule and Thevenin (Figure 7 in [9]) (Figure S1) or of MNHN TAR 1270, although reconstructed (Figure S4), and more similar to that of the specimen shown in Boule and Thevenin (Figure 8 in [9]). The difference between their Figures 7 and 8 might represent sexual dimorphism or ontogeny. It may be impossible to estimate whether Figure 7 represented an even older individual than NMSU 15722 or MNHN TAR 1270, since the Figure 7 specimen lacks molars.

The intermolar distance of the palate widens rostrally in NMSU 15722, whereas it is parallel in MNHN TAR 1270.

The nuchal fossa of NMSU 15722 is deeper, more clearly defined, and occupies more of the vertical height of the reconstructed occiput than that of MNHN TAR 1270 (Figure S4).

MACN Pv 1891 and an unnumbered specimen in the Museum für Naturkunde, Berlin (Figures 2c and 3b, resp., in [32]) exhibit widely separate right and left round external nares separated by a robust ethmoid. The infranasal fossae are also very deep and widely separated. Neither the external nares nor the infranasal fossae appear to be widely separated in NMSU 15722. But the nasal process is damaged, and the ethmoid is mostly missing. The tusks of MACN Pv 1891 appear to be widely divergent and not parallel distally, unlike most other Tarija specimens.

5.2. Compared with Rhynchotherium

Notwithstanding the differences noted above (Section 3.6), LVNHM 871 is similar to NMSU 15722 and unlike *Cuvieronius hyodon*, MNHN TAR 1270, and MACN Pv 1891, in that it exhibits a uniformly narrow gap between the right and left premaxillae and

maxillae, the alveolar margin of the tusks is sharply angled laterally, and the premaxillae and maxillae are blunt-ended rostrally (Figure S3), but not so much as NMSU 15722. If these characters represent intraspecific variation in *C. hyodon*, then they are more likely related to sex than to ontogeny (Section 6, below). Moreover, LVNHM 871 is fully adult and probably female. Regardless, the similarity of NMSU 15722 and LVNHM 871 is testimony to the sister relationship of *Rhynchotherium* and *Cuvieronius* [29], although their similarity could equally result from the retention of primitive characters in *Cuvieronius* if alternative phylogenetic reconstructions are correct [39]. The external nares of LVNHM 871 is much more open and broader laterally than that of NMSU 15722.

5.3. Compared with Gomphotherium

Compared to the skull of *Gomphotherium* (e.g., Figures 366 and 370 in [40]), the skull of *Cuvieronius* has a much broader and more massive rostrum, with root tusks that are relatively much larger than those of *Gomphotherium*. As was pointed out by Osborn (p. 546 in [40]), the skull of *Cuvieronius* is much more similar to that of *Gomphotherium* than to the skulls of *Stegomastodon* and *Notiomastodon* (also see Figures 2–4 in [9]). Thus, the low skull profile, without upward flexure of the face and braincase, is a primitive feature of *Gomphotherium* and *Cuvieronius*, unlike the "flexed" or "elephantoid" skulls of *Stegomastodon*, *Notiomastodon*, and *Rhynchotherium*, in which the highest point of the dorsal surface of the skull is rostral to the nuchal crest rather than the nuchal crest itself. What creates the high-vaulted "elephantoid" skull of many proboscideans is the upward flexure of the face and the braincase above the cheek tooth row (e.g., [40–42]). In true elephants, the longitudinal axis of the alveoli of the tusks projects downward relative to the plane of the occlusal surface of the molars or the alveolar surface of the maxilla (Table 2).

6. Sex Determination

It is difficult to infer the sex of NMSU 15722 with any degree of certainty. Of the very few skulls of *Cuvieronius* that exist with which it can be compared, all are from younger South American deposits and, therefore, necessarily represent a genetically distinct population in which only the largest and oldest individuals can themselves be confidently inferred to be males. Intraspecific polymorphism in the skulls of extant elephantids is profound, e.g., whereby tusk size or even loss is evinced by poaching to be a heritable trait that has been selected against at the population level [43,44]. To the extent to which extant elephants can be inferred as models, interfamilial comparisons must be made with an unknown degree of uncertainty.

The aforementioned notwithstanding, some relevant observations can be made. Foremost, NMSU 15722 was a fully adult individual, as evidenced by fully fused sutures of the dorsal neurocranium and at least some occlusal wear of M3. It can be assumed that it would not likely have grown very much larger and at least approximates the fullest manifestation of its sex.

Tassy [45] inferred sexual dimorphism in the skull of Miocene *Gomphotherium angustidens* to be very similar to that seen in extant *Loxodonta* and *Elephas*. Thus, larger skulls inferred to be those of males have a relatively broad face and a long rostrum. Osborn (Figure 507 in [40]) inferred similar sexual dimorphism in the skull of *Cuvieronius*. He identified a large skull with a wide face and relatively long rostrum (Figure 1 of pl. 1 in [8]) as male, whereas he identified a smaller skull with smaller tusks from the same sample with a narrower face and relatively shorter rostrum (Figure 2 of pl. 1 in [8]) as a female. This suggests that the neotype skull of *Cuvieronius hyodon* MNHN TAR 1270 from Tarija, Bolivia, was a male. We estimate the length of its cranium to be approximately 94 cm, as measured from figures (Figure 1 of pl. 2, Figure 1 of pl. 3 in [9]). The cranium of NMSU 15722 is

approximately 94 cm as well. Cisneros [46] inferred as much as a 30% size difference among *Cuvieronius* from El Salvador by the comparison of a small, fully adult, complete mandible and a much larger mandible of an immature individual, concluding these to be female and male, respectively. Taken at face value, the size of NMSU 15722 might suggest that it was a male. Nevertheless, there appear to be significant differences in the robustness of the MNHN TAR 1270 and NMSU 15722 that call this interpretation into question.

MNHN TAR 1270 is much stockier and more robust than NMSU 15722. This perception could be due in part to differences in the angle at which the dorsal and ventral photographs were taken. It appears as though MNHN TAR 1270 may have been oriented with the tusks tipped more ventrad in Boule and Thevenin (Figure 1 of pl. 3 in [9]) than NMSU 15722 (Figures 3 and 5) because the entire rostral face of the premaxillary alveoli of MNHN TAR 1270 is visible, among other characters. Nevertheless, it is difficult to dismiss the magnitude of these differences as anything but real.

Among the differences that could be affected by the angle of view, the rostral-most width of the premaxillae and bizygomatic width relative to the maxillary constriction or to the overall length of the cranium appear to be much broader in MNHN TAR 1270 than NMSU 15722, lending a much more hourglass-like appearance.

The internal nares of MNHN TAR 1270 appear to be much more caudal (and wider); the extent of its maxillae and palatines caudal to the molars is longer despite the fact that M3 is fully erupted in both NMSU 15722 and MNHN TAR 1270, and the contour of the occiput is more rounded and the exoccipitals thinner in MNHN TAR 1270.

Other differences could simply be due in part to erroneous reconstruction. The zygomatic arches are considerably divergent caudally in MNHN TAR 1270, but they would have been more nearly uniformly parallel if both were preserved in NMSU 15722. The caudal-most extent of the zygomatic processes of the temporal bones is wider than the retroarticular processes of the temporal or exoccipital bones (i.e., lateral-most portion of the occiput/nuchal crest) in MNHN TAR 1270 (Figure 1 of pl. 3 in [9]) (Figure S4), whereas the zygomatic processes are bilaterally narrower than the retroarticular processes in NMSU 15722.

In addition to the aforementioned, caveats notwithstanding, the narrow gap between the premaxillae and the rounder and narrower occipital profile of NMSU 15722 compared to the presumptive male neotype of *C. hyodon*, MNHN TAR 1270, from Tarija, might suggest that NMSU 15722 may have been female, despite their equal size. As noted above, a specimen identified as a juvenile shares the widely separate external nares and divergent premaxillae with those of fully adult specimens ([9], Figure 3B in [32]), and so, these features are inferred to not be related to ontogeny. Thus, we posit that these characters could be related to sexual dimorphism. In contrast, photos and videos of specimens on display in the Museo Nacional de Paleontología y Arqueología in Tarija, Bolivia [24,35,36,47–51] show specimens with a narrow gap between the premaxillae and more cylindrical tusks than those of the neotype of *Cuvieronius hyodon* (Figure 3A,B, pls. 1–3 in [9]) and MACN Pv 1891 (Figure 1 in [52]; Figure 3 in [53]). Unfortunately, we were unable to obtain additional information about any of these specimens and other specimens, with images accessed online as of December 2025.

7. $^{40}Ar/^{39}Ar$ Age Determination

The majority of the 140 dated DS grains are Pleistocene, with the youngest 82 dates yielding an inverse variance-weighted mean age of 1.252 ± 0.003 Ma (Figure 12, Table 3, Supplement S2). Several grains are slightly older and range up to ca. 2 Ma (Figure 12). The K/Ca values range between ~5 and 80 and are typical of sanidine. Other grains fall between about 20 and 40 Ma, with the oldest dates between 60 and 90 Ma (Figure S5).

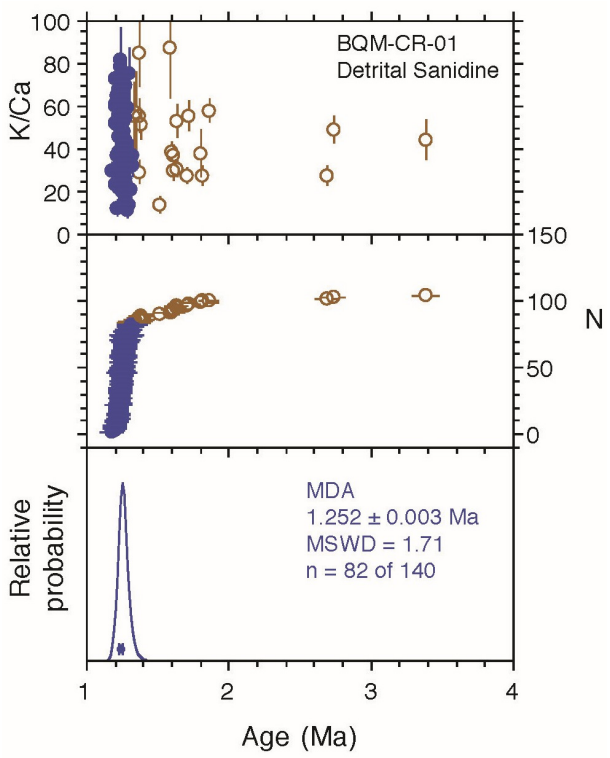


Figure 12. Relative age probability, number of analyses (N), and K/Ca diagrams for detrital sanidine data from sample BQM-CR-01. Data are plotted for dates less than 4 Ma with solid blue symbols representing 82 of the 140 grains that yield a maximum depositional age (MDA) of 1.252 ± 0.003 Ma. Open brown symbols are dates not included in the MDA calculation. MDA is shown with y and x axis error bars below relative probability curve.

Table 3. Summary of detrital sanidine $^{40}Ar/^{39}Ar$ results.

					MDA		
Sample	**L#**	**Irrad**	**Analysis**	**N of N**	**MSWD**	**K/Ca ± 1 s**	**Age (Ma) ± 1 s**
BQM-CR-01	70501	NM-328A	WMA	82 of 140	1.7	44 ± 19	1.252 ± 0.003

Notes: L#—lab identifier; Irrad—Irradiation identifier; N of N—number of dates for MDA of number of total dates; WMA—Inverse variance-weighed mean of selected dates; MDA—Maximum depositional age.

8. Stable Isotope Analysis

The enamel sample of NMSU 15722 returned a $\delta^{13}C$ value of −10.1 ‰, indicating that the individual was predominantly a browser. Three additional samples of dentine yielded an average $\delta^{13}C$ value of −9.5 ‰.

9. Discussion

9.1. $^{40}Ar/^{39}Ar$ Age Determination

The Pleistocene DS dates from BQM-CR-01 are consistent with being derived from the Jemez Volcanic Field (JFV) of Northcentral New Mexico that erupted from the Valles Caldera. Nasholds and Zimmerer [54] report an eruption age of 1.2319 ± 0.0013 Ma (2σ) for the large volume Tshirege eruption that is slightly younger than the maximum depositional age (MDA) of 1.252 ± 0.003 Ma (1σ) reported here. The dated DS grains were not selected to be free of melt inclusions that can contain excess argon (cf. [54]), and thus, despite the slightly older age, we interpret that the DS grains are ultimately derived from the Tshirege eruption. The dates between about 1.3 and 2 Ma are likely a combination of Tshirege grains that are enriched in melt inclusions and/or derived from older JVF rocks. The high concentration of Tshirege grains indicates a significant tephra component to BQM-CR-01

and suggests that the MDA closely approximates the depositional age of BQM-CR-01. If the actual depositional age is substantially less than the MDA, the DS age distribution would likely be much more cosmopolitan as the Rio Grande flows through numerous volcanic units that range between ca. 5 and 40 Ma, and these sanidine ages are quite sparse compared to the large number of Tshirege grains.

9.2. Stable Isotope Analysis

Analysis of carbon and nitrogen isotopes from animal tissues has provided ecologists and paleontologists with a powerful tool to reconstruct diets and foraging niches [55]. Plants employing the C3 photosynthetic pathway are distinct from C4 plants in the relative ratio of ^{13}C to ^{12}C isotopes in their tissues. C3 plants exhibit $\delta^{13}C$ values that vary between −37‰ and −20‰, while C4 plants vary from −16‰ to −10‰. Herbivores acquire the isotopic signatures of their diets with some tissue-specific differences due to fractionation. Consequently, herbivore species can be placed along a trophic continuum from grazers (C4 signatures) to browsers (C3 signatures).

For paleontological analysis, the most common tissue analyzed is tooth enamel. Tooth enamel typically exhibits a strong degree of fractionation that shifts carbon isotopic signatures by approximately +14‰ [56]. Accordingly, Cerling et al. [57] suggested the following demarcations for niche assignments of herbivores based on carbon isotopes of tooth enamel: browsers ($\delta^{13}C \leq -8.0$‰), mixed diet (-8.0‰ $< \delta^{13}C < -1.0$‰), and grazers ($\delta^{13}C \geq -1.0$‰).

Our measured $\delta^{13}C$ value of −10.1 ‰ indicates that NMSU 15722 was predominantly a browser. Notably, it was more of a browser than its C4-consuming contemporaneous conspecifics in sea-level Florida and Texas (Figure 13) [58]. This might reflect differences in dietary availability related to altitude, paralleling those of *Cuvieronius* in the Andes and *Notiomastodon* in the eastern lowlands of South America [59,60] since the elevation of the NMSU 15722 site is 1268 m. Younger North American *Cuvieronius* exhibited a considerably wider range of C3, C4, and mixed diets, possibly reflecting changes in climate, competitive exclusion by mammoths and/or *Stegomastodon* [61], or it may be that older isotope analyses may have been compromised by diagenetic isotope contamination [62,63], although this is less of an issue for carbon isotopes than for S, O, Sr, and other trace elements [63,64]. Among the younger, more variable isotope data reported [58], only four isotope values equaled or were more C3-dominated than that of NMSU 15722. All of them were collected from elevations below 100 m. So, unlike the elevational or latitudinal explanation for differences in dietary isotope differences in South American gomphotheres [65], temperature-mediated differences in forage availability cannot explain the reported variation in isotope values from North America [58].

Previous isotopic analyses of tooth enamel in *Cuvieronius* have yielded mixed results when considering North, Central, and South America combined. For example, a number of studies have identified *Cuvieronius* as a browser [59,60,66], while others suggest a mixed diet [61,66–69]. Interestingly, Pérez-Crespo et al. [66] document a geographic variation in the foraging strategy in some populations of *Cuvieronius*, with some identified as browsers and others as mixed feeders. Taken together, these studies indicate a rather plastic and opportunistic foraging niche for *Cuvieronius*. This has been suggested as a reason why gomphotheres, but not mammoths, may have succeeded in entering South America during the Great American Biotic Interchange (GABI) [66].

9.3. Dental Morphology and Feeding Ecology

Notwithstanding the osteological disparities noted above that cannot be distinguished from individual or even interspecific variation, the dental morphology of *Cuvieronius* was

highly polymorphic [70]. Nevertheless, it remained remarkably stable through time in comparison to the proliferation of lophs and trefoil complexity in the presumptive anagenic evolution of *Stegomastodon primitivus* to *S. mirificus* [71]. This is consistent with the thesis that *Cuvieronius* was a dietary generalist, at least compared to more C3-specialized *Mammut* and C4-specialized *Mammuthus* [58,61]. However, dental morphology may not always accurately reflect feeding ecology [59]. Ideally, we would independently corroborate a temporal shift in diet in *Stegomastodon* but not *Cuvieronius* in support of our proposal. Unfortunately, contemporaneous age-calibrated isotopic data are apparently not available for the relevant time frame of these two genera. Nevertheless, the largely allopatric distribution of the latter South American *Cuvieronius* in the Andean corridor and *Notiomastodon* in the eastern plains [36] (but see [72]) is suggestive of parallel dietary differences between *Cuvieronius* and *Stegomastodon* in North America and between *Cuvieronius* and *Notiomastodon* in South America. Thus, just as *Cuvieronius* is hypothesized to have been competitively excluded by *Mammuthus*, which could monopolize grasslands as the climate warmed in North America [61], *Cuvieronius*, a generalist with less-specialized molar morphology, may have been ill-prepared to compete with *Notiomastodon* in grassland habitats outside of mixed forests of South America. If this analogy is logical, then it is consistent with our observation that the molar morphology of *Cuvieronius*, while heterogeneous, was stable through time. However, it does not explain why *Stegomastodon* and *Cuvieronius* may have differed in their respective abilities to adapt to climate change.

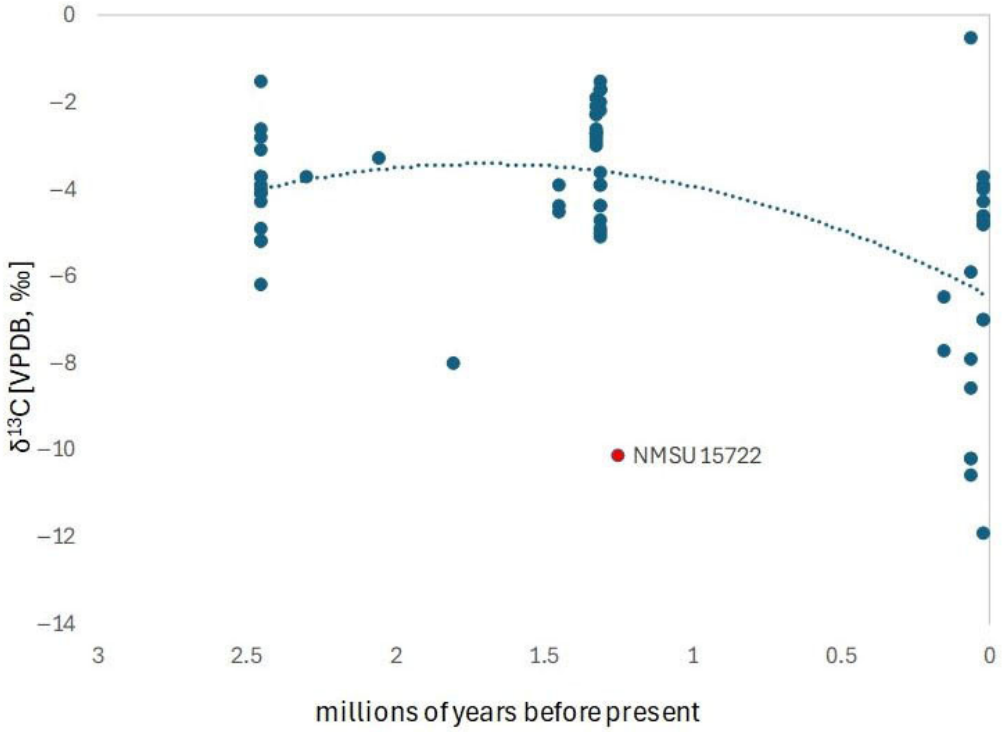


Figure 13. Bivariate graph of $\delta^{13}C$ stable isotope values of North American *Cuvieronius* as a function of time. NMSU 15722 (red circle) is added to the data set of Pardi and DeSantis [58]. Note large residual of NMSU 15722 from regression (dotted) line (correlation by Spearman's rho p (2-tailed) = 0.0046). Second-order regression chosen based on coefficient of determination (R^2 = 0.3115, second-order versus R^2 = 0.1787 linear).

9.4. Taxonomic Assignment

Cuvieronius had been variously described as one of either two or even three or more species from Southern North America, Mesoamerica, and the Andes of South America (reviewed by [70,73,74]). Moreover, the history of nomenclatural and taxonomic revisions of

Cuvieronius is particularly long and confusing [37,75]. The species *C. tropicus* was erected for specimens solely from North and Central America, while those from South America were considered to be *C. hyodon*. Ultimately, all of the species of *Cuvieronius* were synonymized as *C. hyodon* because they are not consistently morphologically distinguishable from one another [71,76]. Thus, *C. hyodon* is currently the only recognized species of *Cuvieronius* [37]. Herein, we resurrect the taxon *C. tropicus* in favor of a biological recognition of cryptic species over a typological definition that prioritizes morphology.

The excavations at Tarija have produced numerous cranial specimens of *Cuvieronius*, exhibiting a broad polymorphism typical of Proboscidea, which presumably largely reflects differences in ontogeny and sex [8,9]. Although the neotype of *Cuvieronius hyodon* (MNHN TAR 1270) appears to be complete as figured (Figure 1 in [7]; pls. 1–3 in [9]), an unknown amount of the skull is reconstructed (Figure S4). In contrast, MACN Pv 1891 appears to be a complete skull (Figure 2C in [32]; Figure 1 in [52]; Figure 3 in [53]), but we have not examined it firsthand. Mothé and dos Santos Avilla [30] list seven additional skulls from Tarija (MNPA-V 006194, MNPA-V 005844, MNPA-V 005799, MNPA-V 005794, MNPA-V 005800, MNPA-V 005810; MACN 1891) that we were unable to examine, and one more allegedly from La Huaca, Piura, Peru (MUSM-Ncn), the existence of which we could not verify. Despite our efforts, we are unable to access documentation (i.e., [77–79], as cited by [80]) of potentially better-preserved alleged continued discoveries over the last century in the Tarija Valley, Bolivia, from where *Cuvieronius* is best known. Still other specimens may be deposited in small collections without having been either published or referenced in online specimen databases. It is for this reason that we believe it is important to document NMSU 15722 here. (Note that the cast of NMSU 15722 on public display at New Mexico State University is slightly remodeled and articulated with the mandible modeled from the cast of a similarly molar-aged specimen.)

NMSU 15722 is the first complete skull of *Cuvieronius* recovered from North or Central America of which we are aware. All other known cranial specimens originate from South America, and they differ morphologically to various degrees in at least some respects. Proboscideans are notoriously polymorphic. Presumptive *C. tropicus* from North America and *C. hyodon* from South America exhibit overlapping variation in the number of molar lophs and trefoil complexity, rendering them morphologically undiagnosable [70,71,76]. Thus, NMSU 15722 cannot be confidently diagnosed as a species distinct from the only few known partial skulls of its South American relatives on morphological criteria. Nevertheless, it most likely represents a genetically different species.

Cryptic sister species may evolve in concert with geophysical barriers and bioclimatic or biogeographic zonation [81]. They may remain morphologically similar due to the recency of divergence or an ecological selective constraint. A substantial percentage of the world's genetically distinct nominal biodiversity may remain undescribed because species are traditionally recognized and described on the typological concept of morphological recognition [82]. This practice is necessarily pervasive in paleontology [83]. But paleontology has evolved from a branch of typological geology into one in which fossils are recognized as biological entities that happen to be extinct [84]. Such is the concept of uniformitarianism, born in geology [85], i.e., that the processes of today are the same as those of the past and can therefore be used to understand the past, and so eloquently extended to evolutionary biology by Charles Darwin [86]. Thus, technologies and principles that are used to understand biological properties of neotaxa can, in some cases, be applied to paleotaxa as well (e.g, [87–93]).

The respective biogeography of North/Central American and South American *Cuvieronius* suggests genetic differentiation warranting recognition as cryptic species. Cryptic species may at times be distinguished by their geographic distribution [94].

North/Central American *Cuvieronius* and Andean *Cuvieronius* are believed to have been fully allopatric, disjunct by ~1000 km, at least during later times for which there is coeval fossil evidence [70].

Of course, "absence of evidence is not evidence of absence." There can be no doubt that gomphotheres traversed this gap at some point in time when they emigrated from Central to South America during GABI. Moreover, 1000 km is within the extreme seasonal migratory range of at least one other proboscidean [95].

Even if the populations were not fully allopatric, then the founder effect [96–99] and isolation by distance [100,101] would both be in play.

South American *Cuvieronius* would have been subject to the founder effect or serial founder effect, most convincingly documented in humans [102–104], considering the complex evolution of the Isthmus of Panama [105–108] and montane barriers and filters to dispersal in Pio-Pleistocene Columbia [109,110]. Founding populations carry only a subset of the total genetic variation present in their source population (i.e., reduced effective population size, Ne). Ne is inversely correlated with the rate and magnitude of genetic drift, the driver of peripatric speciation. Most rare alleles will not be represented, but those that are will be over-represented. Although initially similar to the founding population due to common alleles, heterozygosity is rapidly diminished. Its rate of recovery is inversely correlated with the intrinsic population growth rate (r) [111], which is low in extant proboscideans [112–114]. Genetic divergence equivalent to subspecies has been documented to have evolved in as little as 125 years in replicate fully allopatric founding populations of mynahs [115]. Mynahs have a 3.2-year generation time [116], whereas that of savannah elephants is 25 years [117], and that of mammoths was estimated to have been 15 years [118]. Even this ten-fold difference in generation length suggests a rate of evolution of *Cuvieronius* that falls well within the million-year difference in time between NMSU 15722 and both younger *C. tropicus* and *C. hyodon*.

Sufficient time had elapsed since the formation of the Isthmus at 2.8 Ma [107], or much earlier by other accounts [105,106,108,119], for population divergence, particularly among much younger South American *Cuvieronius* found in an archaeological context [68,120], as well as in North America [121]. Proboscideans are known by 560 ± 40 Ka, and are possibly as old as 2.5 Ma from deposits as far south as Argentina [72,122]. For comparison, early Pleistocene (2.6 Ma to 780 Ka) woolly mammoth mtDNA haplotypes are distinct from those of middle (780 to 126 Ka) and late Pleistocene woolly mammoths [92]. Any introgression between North/Central and South American *Cuvieronius* via an expanded land connection via the Isthmus of Panama (e.g., [70]) would be mollified as described by the isolation by distance model of gene flow [100]. It has even been suggested that Central America was a "center of diversification" of proboscideans [123].

The rate of immigration of *Cuvieronius* cannot be known, but it can be informed by the maximum distances traveled by other proboscideans. The maximum distances traveled by extinct proboscideans, ostensibly immune from the anthropogenic impediments to dispersal faced by extant elephants, have been objectively estimated using $^{87}Sr/^{86}Sr$ strontium, S, and O isotopes. Maximum travel distances in mastodons are estimated to be 150–700 km and anywhere from <200 km [124–126] to as much as 500–1000 km for mammoths employing $^{87}Sr/^{86}Sr$ strontium isotopes [95,127,128].

Studies of mammoth genetics are particularly germane to our thesis. Although woolly mammoths originated in Siberia before crossing the Bering Land Bridge to enter North America [92,129], immigration was reversed in later times and associated with apparent founder effects of 1D and 1E mitochondrial (mtDNA) haplogroups in Eurasia [118,130]. Genetic distances among clade 1 woolly mammoth haplogroups across North America conform to the model of isolation by distance [131]. Most compelling of all,

Arrieta-Donato et al. [131] found deep mtDNA genetic divergence between North American Columbian mammoths and those of the Mexico Central Basin. Northern Columbian mammoth mtDNA haplogroups cluster most closely with 1C mammoths, consistent with the hybrid origin of the species. In contrast, Columbian mammoths of the Mexico Central Basin form the highly divergent 1G haplogroup. Whether or not their genetic distance amounts to the level of interspecific divergence, the pattern is consistent with that of cryptic species. Whether isolation by distance or selection due to environmental differences drove this divergence is a matter of speculation, but it is clear that it transpired over a great amount of time. The divergence of Columbian mammoth mtDNA lineages may be more ancient than the first record of mammoths in North America [92,129,131,132].

Mastodons, too, show evidence of substantial mtDNA divergence in North America. Small founding populations that repeatedly invaded high latitudes during interglacial periods are characterized as having had low levels of genetic diversity [133].

There are caveats to the interpretation of mtDNA studies. Estimates of phylogeny, evolutionary rate (hence, divergence time estimates), and effective population size may differ between mtDNA and nuclear DNA (nDNA) because mtDNA is a non-recombining maternally inherited haplotype that is potentially subject to sexual differences in demography, dispersal, and reproductive variance (e.g., [134,135]). As a single linkage group, mtDNA cannot record gene flow and admixture like nDNA. For example, mtDNA differentiation but no significant nDNA differentiation was found in a continuous savannah elephant population spanning ~470 km [136]. Reconstructing the phylogeny, divergence times, demographics, and phylogeographic history of mtDNA haplogroups can be messy and subject to multiple interpretations and wide confidence intervals, given different assumptions and methods of analysis, without even considering the introgression of mtDNA haplotypes due to hybridization among species [137]. Potentially misleading vagaries of lineage sorting [138] could be fixed more rapidly by 25% smaller Ne of mtDNA, even if the opportunity for polymorphism persistence, hence incomplete lineage sorting, is lower than in nDNA [139]. Small Ne can also yield discordant coalescence times [140].

Sufficient time would appear to have elapsed for species-level genetic divergence to have occurred between 1.2 Ma NMSU 15722 and allopatric late Pleistocene *Cuvieronius hyodon* from South America. The age of *Cuvieronius*-bearing Levels MS-F2 to F9 at the Monte Sur site and levels F2–F5 at the Rujero site in the Tarija–Padcaja Basin, from which the neotype of *Cuvieronius hyodon* probably originated, is 20,840 ± 100 to >39,880 ^{14}C radiocarbon years [141]. *Cuvieronius* is dated to deposits as young as ca. 11,380 ± 320 to 10,190–9700 ^{14}C radiocarbon years in Taguatagua, Chile [142]. The estimated coalescence (most recent common haplotype ancestor) of all Columbian mammoths was 416–307 Ka, and the divergence of all combined North American *M. primigenius* and *M. columbi* haplogroups was 436–323 Ka [131]. While the maximum genetic divergence between the northerly and Mexico Basin Columbian mammoths was insufficient to warrant their designation as distinct species, the timeframe was much shorter than the >1 Ma difference in ages of NMSU 15722 and Tarija *Cuvieronius* (supplementary materials in [131]). This time interval would appear to be unrealistic for the longevity of a chronospecies. Moreover, there is no obvious evidence to suggest that Columbian mammoths experienced a geophysically mediated bottleneck like the Isthmus of Panama. However, the prevalence of gene tree discordance across taxonomic levels due to incomplete lineage sorting or other sources [143] is evidence that fixation can be slow to result in reciprocal monophyly (reviewed by [144]).

Pumas (*Puma concolor*) provide a counter-example to the notion that the biogeography of pan-American large mammals necessarily reflects different species. While as many as 16 mtDNA haplogroups fall into three major clades corresponding to North, Central, and South America, respectively, all are still considered conspecific subspecies [145]. On the

other hand, northerly subspecies exhibit genetic signatures of having experienced a founder effect, emigrating from South America on a much more recent timescale of 10 Ka [146].

In an ironically reverse scenario, extant forest and savannah elephants are morphologically and behaviorally distinct and are estimated to have diverged 4 Ma ago. Yet, convincing evidence for their status as separate species came only from genetic data [147].

10. Conclusions

We describe the first known complete cranium of *Cuvieronius* from North America, dated to the early Irvingtonian, ca. 1.2 Ma. The cranium is of an adult, based on molar eruption and wear. Despite its large size in comparison to other skulls of *Cuvieronius* for which measurements are available, its sex remains ambiguous. It differs in some details from better-known younger Andean populations. We argue that North/Central American and South American *Cuvieronius* are most logically two genetically distinct cryptic species based on >1 Ma differences in age and our inferences about genetic divergence arising from an initial founder effect during the GABI and/or isolation by distance followed by allopatry over a long timescale.

Supplementary Materials: The following supporting information can be downloaded at https://www.mdpi.com/article/10.3390/d18020092/s1: Supplement S1: Supplementary Figures S1–S5. Figure S1: *Cuvieronius* cf. *tropicus* NMSU 15722, subsequent to damage to frontal bones but ostensibly (but unverifiably) preserving the contour of the nuchal region, the outline of which is manually highlighted with stippling; Figure S2: *Rhynchotherium* cf. *falconeri*, cast of LVMNH 871, right lateral view. Note the elevated dorsum of the cranium rostral to the nuchal crest, like that of *Notiomastodon* and *Stegomastodon*, combined with the low supraorbital region and low angle of the tusk relative to the occlusal surface of the molars, like that of *Cuvieronius* and *Gomphotherium*; Figure S3: *Rhynchotherium* cf. *falconeri*, LVMNH 871, on public display in the Las Vegas Museum of Natural History, Nevada, USA, rostral view. Light colored parts are reconstructed. Characters similar to or reminiscent of *Cuvieronius* include the long narrow gap between premaxillae, rostrolaterally facing alveolar margins, lack of a well-defined rostral margin of the external nares laterally, caudally deep and well-defined "incisive fossa" (sensu [30]) that terminates in deep but reconstructed "infranasal fossae" (our terminology). The domed "forehead", broad and cavernous external nares, and presence of lower incisors distinguish *Rhynchotherium* from *Cuvieronius*; Figure S4: *Cuvieronius hyodon* MNHN TAR 1270 neotype on public display in the Muséum national d'Histoire naturelle in Paris, France. Differences in color and surface texture are evidence of reconstruction of the left and medial right premaxillae, frontal, parietal, nuchal, and zygomatic regions. A, rostral aspect; B, caudal aspect; C, right lateral aspect; D, left lateral aspect. Images not to scale; Figure S5: Relative age probability, number of analyses (N) and K/Ca diagrams for all detrital sanidine data from sample BQM-CR-01. Supplement S2: Detrital sanidine $^{40}Ar/^{39}Ar$ data. Sheet S1: Summary of $^{40}Ar/^{39}Ar$ results; Sheet S2: Age and ratio data; Sheet S3: Argon intensity data.

Author Contributions: Conceptualization, P.H.; methodology, P.H., S.G.L., M.H., J.R., W.J.B. and B.H.; validation, P.H., S.G.L., M.H. and J.R.; formal analysis, P.H., S.G.L. and J.R.; investigation, P.H., S.G.L., M.H., J.R. and W.J.B.; writing—original draft preparation, P.H., S.G.L., M.H. and W.J.B.; writing—review and editing, P.H., S.G.L., M.H. and J.R.; visualization, P.H., S.G.L. and M.H.; supervision, P.H.; project administration, P.H.; funding acquisition, P.H. All authors have read and agreed to the published version of the manuscript.

Funding: This work was supported by NMSU and by a private donation from Michael Johnson.

Data Availability Statement: The original contributions presented in this study are included in the article/Supplementary Material. Further inquiries can be directed to the corresponding authors.

Acknowledgments: We are grateful to Eddie Binns for donating NMSU 15722 to the Vertebrate Museum of NMSU and for providing a heavy excavator. We are also indebted to Bethany Cook for

performing the stable isotope laboratory analysis. Rob Gaston kindly molded and cast the specimen. We appreciate the efforts of two anonymous reviewers who made helpful suggestions that improved the content and clarity of the manuscript.

Conflicts of Interest: The authors declare no conflicts of interest.

References

1. Tedford, R.H. Mammalian Biochronology of the Late Cenozoic Basins of New Mexico. *Geol. Soc. Am. Bull.* **1981**, *92*, 1008. [CrossRef]
2. Vanderhill, J.B. Lithostratigraphy, Vertebrate Paleontology, and Magnetostratigraphy of Plio-Pleistocene Sediments in the Mesilla Basin, New Mexico. Ph.D. Thesis, University of Texas, Austin, TX, USA, 1986.
3. Harris, A. *Pleistocene Vertebrates of Arizona, New Mexico, and Trans-Pecos Texas*; UTEP Biodiversity Collections, Centennial Museum, and Department of Biological Sciences, University of Texas at El Paso: El Paso, Texas, 2012; pp. 1–1631. Available online: https://www.researchgate.net/publication/236842872_Pleistocene_Vertebrates_of_Arizona_New_Mexico_and_Trans-Pecos_Texas (accessed on 18 December 2025).
4. Morgan, G.S.; Harris, A.H. Pliocene and Pleistocene Vertebrates of New Mexico. *N. M. Mus. Nat. Hist. Sci. Bull.* **2015**, *68*, 233–427.
5. Mack, G.H.; Salyards, S.L.; James, W.C. Magnetostratigraphy of the Plio-Pleistocene Camp Rice and Palomas Formations in the Rio Grande Rift of Southern New Mexico. *Am. J. Sci.* **1993**, *293*, 49–77. [CrossRef]
6. Mack, G.H.; Seager, W.R.; Leeder, M.R.; Perez-Arlucea, M.; Salyards, S.L. Pliocene and Quaternary History of the Rio Grande, the Axial River of the Southern Rio Grande Rift, New Mexico, USA. *Earth-Sci. Rev.* **2006**, *79*, 141–162. [CrossRef]
7. Lucas, S.G. Case 3479 *Cuvieronius* Osborn, 1923 (Mammalia, Proboscidea): Proposed Conservation. *Bull. Zool. Nomencl.* **2009**, *66*, 265–270. [CrossRef]
8. Nordenskiöld, E. *Über Die Säugetierfossilien Des Tarijatals, Südamerika. I Mastodon andium* Cuv. *Proc. R. Swed. Acad. Sci.* **1903**, *37*, 161–166. Available online: http://hdl.handle.net/2027/hvd.32044066263096 (accessed on 18 December 2025).
9. Boule, M.; Thevenin, A. *Mammifères Fossiles de Tarija*; Soudier: Paris, France, 1920; pp. 1–255; pls. I–XXVI. Available online: https://archive.org/details/mammifresfossi00bouluoft/page/n11/mode/2up (accessed on 18 December 2025).
10. Lucas, S.G. Case 3515 *Rhynchotherium* Falconer, 1868 (Mammalia; Proboscidea): Proposed Conservation of Usage by Designation of *Rhynchotherium falconeri* Osborn, 1923 as the Type Species. *Bull. Zool. Nomencl.* **2010**, *67*, 158–162. [CrossRef]
11. Miller, W.E. A *Rhynchotherium* Skull and Mandible from Southeastern Arizona. *Brigh. Young Univ. Geol. Stud.* **1990**, *36*, 57–67.
12. van der Merwe, N.J.; Bezuidenhout, A.J.; Seegers, C.D. The Skull and Mandible of the African Elephant (*Loxodonta africana*). *Onderstepoort J. Vet. Res.* **1995**, *62*, 245–260.
13. Kuiper, K.F.; Deino, A.; Hilgen, F.J.; Krijgsman, W.; Renne, P.R.; Wijbrans, J.R. Synchronizing Rock Clocks of Earth History. *Science* **2008**, *320*, 500–504. [CrossRef]
14. Koch, P.L.; Tuross, N.; Fogel, M.L. The Effects of Sample Treatment and Diagenesis on the Isotopic Integrity of Carbonate in Biogenic Hydroxylapatite. *J. Archaeol. Sci.* **1997**, *24*, 417–429. [CrossRef]
15. Fox, D.L.; Fisher, D.C. Dietary Reconstruction of Miocene *Gomphotherium* (Mammalia, Proboscidea) from the Great Plains Region, USA, Based on the Carbon Isotope Composition of Tusk and Molar Enamel. *Palaeogeogr. Palaeoclimatol. Palaeoecol.* **2004**, *206*, 311–335. [CrossRef]
16. Illiger, J.K.W. *Prodromus Systematis Mammalium et Avium Additis Terminis Zoographicis Utriusque Classis, Eorumque Versione Germanica*; Sumptibus C. Salfeld: Berlin, Germany, 1811; pp. 1–302. Available online: https://www.biodiversitylibrary.org/item/188747#page/7/mode/1up (accessed on 18 December 2025).
17. Hay, O.P. Further Observations on Some Extinct Elephants. *Proc. Biol. Soc. Wash.* **1922**, *35*, 97–101. Available online: https://www.biodiversitylibrary.org/part/6682 (accessed on 18 December 2025).
18. Osborn, H.F. New Subfamily, Generic, and Specific Stages in the Evolution of the Proboscidea. *Am. Mus. Novit.* **1923**, *99*, 1–4. Available online: https://digitallibrary.amnh.org/items/8c56f046-e088-4174-91fe-f9377dac5433 (accessed on 18 December 2025).
19. Cope, E.D. The Extinct Mammalia of the Valley of Mexico. *Proc. Am. Philos. Soc.* **1885**, *22*, 1–21.
20. Hawley, J.W.; Kottlowski, F.E.; King, W.E.; Strain, W.S.; Seager, W.R.; LeMone, D.E. The Santa Fe Group in the South-Central New Mexico Border Region. *Bord. Stratigr. Symp. N. M. Bur. Mines Miner. Resour. Circ.* **1969**, *104*, 52–76.
21. Perez-Arlucea, M.; Mack, G.H.; Leeder, M.R. Reconstructing the Ancestral (Plio-Pleistocene) Rio Grande in Its Active Tectonic Setting, Southern Rio Grande Rift, New Mexico, USA. *Sedimentology* **2000**, *47*, 701–720. [CrossRef]
22. Seager, W.R.; Clemons, R.E.; Hawley, J.W.; Kelley, R.E. Geology of Northwest Part of Las Cruces 1° × 2° Sheet 1982. In *New Mexico Bureau of Mines and Mineral Resources Geologic Map 53, Scale 1:125,000*; New Mexico Bureau of Mines & Mineral Resources: Socorro, NM, USA. [CrossRef]
23. Mack, G.H.; Salyards, S.L.; McIntosh, W.C.; Leeder, M.R. Reversal Magnetostratigraphy and Radioisotopic Geochronology of the Plio-Pleistocene Camp Rice and Palomas Formations, Southern Rio Grande Rift. In *Las Cruces Country II*; Mack, G.H., Austin,

G.S., Barker, J.M., Eds.; New Mexico Geological Society Guidebook, 49th Field Conference, Las Cruces, NM, USA; New Mexico Geological Society: Socorro, NM, USA, 1988; Volume 49, pp. 229–236. [CrossRef]
24. Lucas, S.G.; Morgan, G.S.; Estep, J.W.; Mack, G.H.; Hawley, J.W. Co-Occurrence of the Proboscideans *Cuvieronius, Stegomastodon*, and *Mammuthus* in the Lower Pleistocene of Southern New Mexico. *J. Vertebr. Paleontol.* **1999**, *19*, 595–597. [CrossRef]
25. Morgan, G.S.; Hulbert, R.C.; Gottlieb, E.S.; Amato, J.M.; Mack, G.H.; Jonell, T.N. The Tapir *Tapirus* (Mammalia: Perissodactyla) from the Late Pliocene (Early Blancan) Tonuco Mountain Local Fauna, Camp Rice Formation, Doña Ana County, Southern New Mexico. *N. M. Geol.* **2017**, *39*, 28–39. [CrossRef]
26. Houde, P.; Peltier, D. A New *Stegomastodon* Skull (Proboscidea: Gomphotheriidae) from the Camp Rice Formation, Doña Ana County, New Mexico. In *Las Cruces Country III*; Mack, G.H., Hampton, B.A., Ramos, F.C., Witcher, J.C., Ulmer-Scholle, D.S., Eds.; New Mexico Geological Society Guidebook, 69th Field Conference, Las Cruces, NM, USA; New Mexico Geological Society: Socorro, NM, USA, 2018; Volume 69, pp. 53–56. Available online: https://www.researchgate.net/publication/365333186_A_new_Stegomastodon_skull_Proboscidea_Gomphotheriidae_from_the_Camp_Rice_Formation_Dona_Ana_County_New_Mexico (accessed on 18 December 2025). [CrossRef]
27. Mack, G.H.; McIntosh, W.C.; Leeder, M.R.; Monger, H.C. Plio-Pleistocene Pumice Floods in the Ancestral Rio Grande, Southern Rio Grande Rift, USA. *Sediment. Geol.* **1996**, *103*, 1–8. [CrossRef]
28. Mack, G.; Dunbar, N.; Foster, R. New Sites of 3.1-Ma Pumice Beds in Axial Fluvial Strata of the Camp Rice and Palomas Formations, Southern Rio Grande Rift. *N. M. Geol.* **2009**, *31*, 31–37. [CrossRef]
29. Mothé, D.; Ferretti, M.P.; Avilla, L.S. The Dance of Tusks: Rediscovery of Lower Incisors in the Pan-American Proboscidean *Cuvieronius hyodon* Revises Incisor Evolution in Elephantimorpha. *PLoS ONE* **2016**, *11*, e0147009. [CrossRef]
30. Mothé, D.; dos Santos Avilla, L. Mythbusting Evolutionary Issues on South American Gomphotheriidae (Mammalia: Proboscidea). *Quat. Sci. Rev.* **2015**, *110*, 23–35. [CrossRef]
31. Pidgeon, E. *The Fossil Remains of the Animal Kingdom*; Whittaker, Treacher and Co.: London, UK, 1830; pp. 1–544. Available online: https://archive.org/details/fossilremainsofa00pidg (accessed on 18 December 2025).
32. Prado, J.L.; Alberdi, M.T. A Cladistic Analysis among Trilophodont Gomphotheres (Mammalia, Proboscidea) with Special Attention to the South American Genera. *Palaeontology* **2008**, *51*, 903–915. [CrossRef]
33. Prado, J.L.; Alberdi, M.T. Global Evolution of Equidae and Gomphotheriidae from South America. *Integr. Zool.* **2014**, *9*, 434–443. [CrossRef] [PubMed]
34. Todd, N.E. New Phylogenetic Analysis of the Family Elephantidae Based on Cranial-Dental Morphology. *Anat. Rec.* **2010**, *293*, 74–90. [CrossRef]
35. Martinez Antelo, H. *Cuvieronius* Museo Nacional de Paleontología y Arqueología, Tarija, Bolivia. Available online: https://www.fotopaises.com/foto/tarija-bolivia-bolivia-25566 (accessed on 18 December 2025).
36. Martinez Antelo, H. *Cuvieronius* Museo Nacional de Paleontología y Arqueología, Tarija, Bolivia. Available online: https://www.fotopaises.com/foto/tarija-bolivia-25565 (accessed on 18 December 2025).
37. Lucas, S.G. The Palaeobiogeography of South American Gomphotheres. *J. Paleogeography* **2013**, *2*, 19–40. [CrossRef]
38. Cruz Casso, R. Museo Paleontológico Para La Ciudad de Tarija/Cruz Casso, Raquel/37233_RESUMEN.pdf. 2017. Available online: https://biblioteca.uajms.edu.bo/opac_css/index.php?lvl=search_result (accessed on 18 December 2025).
39. Baleka, S.; Varela, L.; Tambusso, P.S.; Paijmans, J.L.A.; Mothé, D.; Stafford, T.W.; Fariña, R.A.; Hofreiter, M. Revisiting Proboscidean Phylogeny and Evolution through Total Evidence and Palaeogenetic Analyses Including *Notiomastodon* Ancient DNA. *iScience* **2022**, *25*, 103559. [CrossRef]
40. Osborn, H.F. *Proboscidea: A Monograph of the Discovery, Evolution, Migration and Extinction of the Mastodonts and Elephants of the World, Volume I Mœritheroidea Deinotheroidea Mastodontoidea*; The American Museum Press: New York, NY, USA, 1936; pp. 1–802. Available online: https://archive.org/details/proboscideamonog01osbo (accessed on 18 December 2025).
41. Gregory, W.K. Adaptive Significance of the Shortening of the Elephant's Skull. *Bull. Am. Mus. Nat. Hist.* **1903**, *19*, 387–394.
42. Jie, Y.; Wenyu, W.; Hang, J. Reconstruction of the Jaw-Closing Muscles of *Platybelodon tongxinensis* (Amebelodontidae, Proboscidea) and Discussion of Cranial Evolution from Long-Jawed Mastodont to Short-Jawed Elephantid. *Vertebr. Palasiat.* **1990**, *28*, 284–295.
43. Chiyo, P.I.; Obanda, V.; Korir, D.K. Illegal Tusk Harvest and the Decline of Tusk Size in the African Elephant. *Ecol. Evol.* **2015**, *5*, 5216–5229. [CrossRef]
44. Campbell-Staton, S.C.; Arnold, B.J.; Gonçalves, D.; Granli, P.; Poole, J.; Long, R.A.; Pringle, R.M. Ivory Poaching and the Rapid Evolution of Tusklessness in African Elephants. *Science* **2021**, *374*, 483–487. [CrossRef]
45. Tassy, P. Growth and Sexual Dimorphism among Miocene Elephantoids: The Example of *Gomphotherium angustidens*. In *The Proboscidea*; Shoshani, J., Tassy, P., Eds.; Oxford University Press: Oxford, UK, 1996; pp. 92–100.
46. Cisneros, J.C. New Pleistocene Vertebrate Fauna from El Salvador. *Rev. Bras. Paleontol.* **2005**, *8*, 239–255. [CrossRef]
47. Martinez Antelo, H. *Cuvieronius* Museo Nacional de Paleontología y Arqueología, Tarija, Bolivia. Available online: https://www.fotopaises.com/foto/tarija-bolivia-25564 (accessed on 18 December 2025).

48. ibolivia.org Museo Nacional Paleontológico. Available online: https://www.ibolivia.org/museo-nacional-paleontologico-tarija (accessed on 18 December 2025).
49. Museo Nacional de Paleontología y Arqueología, Tarija, Bolivia Museo Nacional de Paleontología y Arqueología, Tarija, Bolivia. Available online: https://munaparq.uajms.edu.bo/exposicion/sala-1/ (accessed on 18 December 2025).
50. Museo Nacional Paleontológico Arqueológico de Tarija Museo Nacional Paleontológico Arqueológico de Tarija. Available online: https://www.ibolivia.org/museo-nacional-paleontologico-tarija (accessed on 18 December 2025).
51. Carrasco Patzi, M.R.; Carrasco, C.C. Museo Nacional de Paleontología y Arqueología, Tarija, Bolivia. Available online: https://www.youtube.com/watch?v=c05axHZ6AAcandt=244s (accessed on 18 December 2025).
52. Alberdi, M.T.; Prado, J.L. Fossil Gomphotheriidae from Argentina. *Historia Evolutiva y Paleobiogeográfica de los Vertebrados de América del Sur Contribuciones del MACN*. 2016, Volume 6, pp. 275–283. Available online: https://www.researchgate.net/publication/324570077_Fossil_Gomphotheriidae_from_Argentina (accessed on 18 December 2025).
53. Mothé, D.; dos Santos Avilla, L.; Asevedo, L.; Borges-Silva, L.; Rosas, M.; Labarca-Encina, R.; Souberlich, R.; Soibelzon, E.; Roman-Carrion, J.L.; Ríos, S.D.; et al. Sixty Years after 'The Mastodonts of Brazil': The State of the Art of South American Proboscideans (Proboscidea, Gomphotheriidae). *Quat. Int.* **2017**, *443*, 52–64. [CrossRef]
54. Nasholds, M.W.M.; Zimmerer, M.J. High-Precision $^{40}Ar/^{39}Ar$ Geochronology and Volumetric Investigation of Volcanism and Resurgence Following Eruption of the Tshirege Member, Bandelier Tuff, at the Valles Caldera. *J. Volcanol. Geotherm. Res.* **2022**, *431*, 107624. [CrossRef]
55. Boecklen, W.J.; Yarnes, C.T.; Cook, B.A.; James, A.C. On the Use of Stable Isotopes in Trophic Ecology. *Annu. Rev. Ecol. Evol. Syst.* **2011**, *42*, 411–440. [CrossRef]
56. Cerling, T.E.; Harris, J.M. Carbon Isotope Fractionation between Diet and Bioapatite in Ungulate Mammals and Implications for Ecological and Paleoecological Studies. *Oecologia* **1999**, *120*, 347–363. [CrossRef]
57. Cerling, T.E.; Andanje, S.A.; Blumenthal, S.A.; Brown, F.H.; Chritz, K.L.; Harris, J.M.; Hart, J.A.; Kirera, F.M.; Kaleme, P.; Leakey, L.N.; et al. Dietary Changes of Large Herbivores in the Turkana Basin, Kenya from 4 to 1 Ma. *Proc. Natl. Acad. Sci. USA* **2015**, *112*, 11467–11472. [CrossRef]
58. Pardi, M.I.; DeSantis, L.R.G. Dietary Plasticity of North American Herbivores: A Synthesis of Stable Isotope Data over the Past 7 Million Years. *Proc. R. Soc. B Biol. Sci.* **2021**, *288*, 20210121. [CrossRef]
59. Sánchez, B.; Prado, J.L.; Alberdi, M.T. Feeding Ecology, Dispersal, and Extinction of South American Pleistocene Gomphotheres (Gomphotheriidae, Proboscidea). *Paleobiology* **2004**, *30*, 146–161. [CrossRef]
60. Pérez-Crespo, V.A.; Laurito, C.A.; Arroyo-Cabrales, J.; Valerio, A.L.; Cienfuegos-Alvarado, E.; Otero, F.J. Feeding Habits of the Gomphothere *Cuvieronius hyodon* in Costa Rica: A Biochemical Approach. *Hist. Biol.* **2024**, *36*, 734–741. [CrossRef]
61. Smith, G.J.; DeSantis, L.R.G. Extinction of North American *Cuvieronius* (Mammalia: Proboscidea: Gomphotheriidae) Driven by Dietary Resource Competition with Sympatric Mammoths and Mastodons. *Paleobiology* **2020**, *46*, 41–57. [CrossRef]
62. Gomes, J.P.B.; Bunevich, R.B.; Sartorato, A.C.L.; Tedeschi, L.R.; Tonietto, S.N.; Tucker, M.E.; Whitaker, F. Early Diagenetic Evolution Based on Petrography and Stable Isotope Analysis in the Barra Velha Formation of the Brazilian Pre-salt. *Depos. Rec.* **2025**, *11*, 70–94. [CrossRef]
63. Stevens, R.E.; Pederzani, S.; Britton, K.; Wexler, S.K. Bones and Teeth Isotopes as Archives for Palaeoclimatic, Palaeoenvironmental and Palaeoecological Data. *Quat. Sci. Rev.* **2025**, *357*, 109320. [CrossRef]
64. Wang, Y.; Cerling, T.E. A Model of Fossil Tooth and Bone Diagenesis: Implications for Paleodiet Reconstruction from Stable Isotopes. *Palaeogeogr. Palaeoclimatol. Palaeoecol.* **1994**, *107*, 281–289. [CrossRef]
65. Domingo, L.; Prado, J.L.; Alberdi, M.T. The Effect of Paleoecology and Paleobiogeography on Stable Isotopes of Quaternary Mammals from South America. *Quat. Sci. Rev.* **2012**, *55*, 103–113. [CrossRef]
66. Pérez-Crespo, V.A.; Prado, J.L.; Alberdi, M.T.; Arroyo-Cabrales, J.; Johnson, E. Diet and Habitat for Six American Pleistocene Proboscidean Species Using Carbon and Oxygen Stable Isotopes. *Ameghiniana* **2015**, *53*, 39–51. [CrossRef]
67. MacFadden, B.J.; Shockey, B.J. Ancient Feeding Ecology and Niche Differentiation of Pleistocene Mammalian Herbivores from Tarija, Bolivia: Morphological and Isotopic Evidence. *Paleobiology* **1997**, *23*, 77–100. [CrossRef]
68. Labarca, R.O.; Lopez, P.G. Los Mamiferos finiPleistocénicos de La Formación Quebrada Quereo (IV Regiónchile): Biogeografía e Inferencias Paleoambi-Entales. *Mastozool. Neotrop.* **2016**, *13*, 89–101.
69. Marín-Leyva, A.H.; Mainou, L.; Perez-Crespo, V.A.; Straulino Mainou, L.; Arreola, I.M.; Solís-Pichardo, G.; Cienfuegos-Alvarado, E.; Alberdi, M.T. The Life Story of a Gomphothere from East-Central Mexico: A Multidisciplinary Approach. *J. S. Am. Earth Sci.* **2021**, *111*, 103442. [CrossRef]
70. Morgan, G.S.; MacFadden, B.J.; Martínez, M. Quaternary Gomphotheres (Mammalia: Proboscidea: Gomphotheriidae) from the Continental Shelf, Pearl Islands, Panama. *Quat. Int.* **2016**, *392*, 335–348. [CrossRef]
71. Lucas, S.G. *Cuvieronius* (Mammalia, Proboscidea) from the Neogene of Florida. *N. M. Mus. Nat. Hist. Sci. Bull.* **2008**, *44*, 31–38.

72. Mothé, D.; Kinoshita, A.; Baffa, O.; Luna, C.A. Doing the Time Warp Again: Electron Spin Resonance Dating Reveals Oldest Numeric Age for *Notiomastodon platensis* Ameghino, 1888 (Mammalia, Proboscidea). *Geobios* **2025**, *91*, 81–88. [CrossRef]
73. Mothé, D.; Avilla, L.S.; Cozzuol, M.; Winck, G.R. Taxonomic Revision of the Quaternary Gomphotheres (Mammalia: Proboscidea: Gomphotheriidae) from the South American Lowlands. *Quat. Int.* **2012**, *276–277*, 2–7. [CrossRef]
74. Mothé, D.; Avilla, L.S.; Cozzuol, M.A. The South American Gomphotheres (Mammalia, Proboscidea, *Gomphotheriidae*): Taxonomy, Phylogeny, and Biogeography. *J. Mamm. Evol.* **2013**, *20*, 23–32. [CrossRef]
75. Lucas, S.G. Taxonomic Nomenclature of *Cuvieronius* and *Haplomastodon*, Proboscideans from the Plio-Pleistocene of the New World. *N. M. Mus. Nat. Hist. Sci. Bull.* **2008**, *44*, 409–415.
76. Lucas, S.G.; Alvarado, G.E. Fossil Proboscidea from the Upper Cenozoic of Central America: Taxonomy, Evolutionary and Paleobiogegraphic Significance. *Rev. Geológica América Cent.* **2010**, *42*, 9–42. [CrossRef]
77. Takai, F.; Arozqueta, B.; Mizuno, T.; Yoshida, A.; Kondo, H. On Fossil Mammals from the Tarija Department, Southern Bolivia. *Res. Inst. Evol. Biol. Tokyo* **1984**, *4*, 1–63.
78. Takai, F.; Mizuno, T.; Iwasaki, Y.; Kotake, T.; Yoshida, A.; Arozqueta, B. Fossil Mammals Excavated in the Tarija Basin, Bolivia. *Res. Inst. Evol. Biol. Tokyo* **1980**, *2*, 1–63.
79. Takai, F.; Mizuno, T.; Iwasaki, Y.; Tanaka, K.; Yoshida, A. Tarija Mammal-Bearing Formation in Bolivia. *Res. Inst. Evol. Biol. Tokyo* **1982**, *3*, 1–72.
80. Ferretti, M.P. A Review of South American Proboscideans. In *Neogene Mammals. New Mexico Museum of Natural Science Bulletin*; Lucas, S.G., Morgan, G.S., Spielman, J.A., Prothero, D.R., Lucas, S.G., Morgan, G.S., Spielman, J.A., Prothero, D.R., Eds.; New Mexico Museum of Natural History and Science: Albuquerque, NM, USA, 2008; Volume 44, pp. 381–391.
81. Kozak, K.H.; Wiens, J.J. Climatic Zonation Drives Latitudinal Variation in Speciation Mechanisms. *Proc. R. Soc. B Biol. Sci.* **2007**, *274*, 2995–3003. [CrossRef]
82. Hending, D. Cryptic Species Conservation: A Review. *Biol. Rev.* **2025**, *100*, 258–274. [CrossRef]
83. Shin, C.P.; Allmon, W.D. How We Study Cryptic Species and Their Biological Implications: A Case Study from Marine Shelled Gastropods. *Ecol. Evol.* **2023**, *13*, e10360. [CrossRef]
84. Allmon, W.D. Studying Species in the Fossil Record: A Review and Recommendations for a More Unified Approach. In *Species and Speciation in the Fossil Record*; Allmon, W.D., Yacobucci, M.M., Eds.; The University of Chicago Press: Chicago, IL, USA; London, UK, 2016; pp. 59–120. Available online: https://books.google.com/books?hl=en&lr=&id=_2cpDQAAQBAJ&oi=fnd&pg=PA59&dq=Studying+species+in+the+fossil+record:+A+review+and+recommendations+for+a+more+unified+approach&ots=OTxGvpoHlr&sig=qdeo-PThhHIzv4caraq_5JwUt6I#v=onepage&q&f=false (accessed on 18 December 2025).
85. Hutton, J.X. Theory of the Earth; or an Investigation of the Laws Observable in the Composition, Dissolution, and Restoration of Land upon the Globe. *Earth Environ. Sci. Trans. R. Soc. Edinb.* **1788**, *1*, 209–304. [CrossRef]
86. Darwin, C. *On the Origin of Species by Means of Natural Selection or the Preservation of Favoured Races in the Struggle for Life*, 1st ed.; John Murray: London, UK, 1859; pp. 1–502. Available online: https://www.gutenberg.org/files/1228/1228-h/1228-h.htm (accessed on 18 December 2025).
87. de Souza Barbosa, F.H.D.S.; Araújo-Júnior, H.I.D.; Mothé, D.; dos Santos Avilla, L. Osteological Diseases in an Extinct *Notiomastodon* (Mammalia, Proboscidea) Population from the Late Pleistocene of Brazil. *Quat. Int.* **2017**, *443*, 228–232. [CrossRef]
88. Bailleul, A.M.; O'Connor, J.; Zhang, S.; Li, Z.; Wang, Q.; Lamanna, M.C.; Zhu, X.; Zhou, Z. An Early Cretaceous Enantiornithine (Aves) Preserving an Unlaid Egg and Probable Medullary Bone. *Nat. Commun.* **2019**, *10*, 1275. [CrossRef]
89. Buckley, M.; Recabarren, O.P.; Lawless, C.; García, N.; Pino, M. A Molecular Phylogeny of the Extinct South American Gomphothere through Collagen Sequence Analysis. *Quat. Sci. Rev.* **2019**, *224*, 105882. [CrossRef]
90. Hsieh, S.; Plotnick, R.E. The Representation of Animal Behaviour in the Fossil Record. *Anim. Behav.* **2020**, *169*, 65–80. [CrossRef]
91. Buchmann, R.; Rodrigues, T. Resistance of Cervical Vertebrae in Response to Muscular Stresses in Pterosaurs: Implications for Foraging Habits and Skeletal Pneumatization. *PeerJ* **2025**, *13*, e20388. [CrossRef]
92. Chacón-Duque, J.C.; Thomas Thorpe, J.A.; Li, W.; Dehasque, M.; Pečnerová, P.; Barlow, A.; Díez-del-Molino, D.; Henneberger, K.; Jin, C.; Moreland, K.N.; et al. A Million Years of Mammoth Mitogenome Evolution. *Mol. Biol. Evol.* **2025**, *42*, msaf065. [CrossRef]
93. Mármol-Sánchez, E.; Fromm, B.; Oskolkov, N.; Pochon, Z.; Dehasque, M.; Aslanzadeh, M.; Bozlak, E.; Brown, K.; Van Der Valk, T.; Kalogeropoulos, P.; et al. Ancient RNA Expression Profiles from the Extinct Woolly Mammoth. *Cell* **2026**, *189*, 52–69.e22. [CrossRef]
94. Gaytán, Á.; Bergsten, J.; Canelo, T.; Pérez-Izquierdo, C.; Santoro, M.; Bonal, R. DNA Barcoding and Geographical Scale Effect: The Problems of Undersampling Genetic Diversity Hotspots. *Ecol. Evol.* **2020**, *10*, 10754–10772. [CrossRef] [PubMed]
95. Rowe, A.G.; Bataille, C.P.; Baleka, S.; Combs, E.A.; Crass, B.A.; Fisher, D.C.; Ghosh, S.; Holmes, C.E.; Krasinski, K.E.; Lanoë, F.; et al. A Female Woolly Mammoth's Lifetime Movements End in an Ancient Alaskan Hunter-Gatherer Camp. *Sci. Adv.* **2024**, *10*, eadk0818. [CrossRef] [PubMed]

96. Mayr, E. Change of Genetic Environment and Evolution. In *Evolution as a Process*; Huxley, J., Hardy, A.C., Ford, E.B., Eds.; Allen & Unwin: London, UK, 1954; pp. 157–180. Available online: https://www.bibsonomy.org/bibtex/10fdc2e4ddded4d1e8f68b37545baa6ca (accessed on 18 December 2025).
97. Templeton, A.R. The Theory of Speciation via the Founder Principle. *Genetics* **1980**, *94*, 1011–1038. [CrossRef]
98. Templeton, A.R. The Reality and Importance of Founder Speciation in Evolution. *BioEssays* **2008**, *30*, 470–479. [CrossRef]
99. Carson, H.L.; Templeton, A.R. Genetic Revolutions in Relation to Speciation Phenomena: The Founding of New Populations. *Annu. Rev. Ecol. Syst.* **1984**, *15*, 97–131. [CrossRef]
100. Wright, S. Isolation by Distance. *Genetics* **1943**, *28*, 114–138. [CrossRef]
101. Relethford, J. Global Patterns of Isolation by Distance Based on Genetic and Morphological Data. *Hum. Biol.* **2004**, *76*, 499–513. [CrossRef]
102. Ramachandran, S.; Deshpande, O.; Roseman, C.C.; Rosenberg, N.A.; Feldman, M.W.; Cavalli-Sforza, L.L. Support from the Relationship of Genetic and Geographic Distance in Human Populations for a Serial Founder Effect Originating in Africa. *Proc. Natl. Acad. Sci. USA* **2005**, *102*, 15942–15947. [CrossRef]
103. DeGiorgio, M.; Jakobsson, M.; Rosenberg, N.A. Explaining Worldwide Patterns of Human Genetic Variation Using a Coalescent-Based Serial Founder Model of Migration Outward from Africa. *Proc. Natl. Acad. Sci. USA* **2009**, *106*, 16057–16062. [CrossRef]
104. 1000 Genomes Project Consortium. A Global Reference for Human Genetic Variation. *Nature* **2015**, *526*, 68. [CrossRef]
105. Woodburne, M.O. The Great American Biotic Interchange: Dispersals, Tectonics, Climate, Sea Level and Holding Pens. *J. Mamm. Evol.* **2010**, *17*, 245–264. [CrossRef]
106. Montes, C.; Cardona, A.; Jaramillo, C.; Pardo, A.; Silva, J.C.; Valencia, V.; Ayala, C.; Pérez-Angel, L.C.; Rodriguez-Parra, L.A.; Ramirez, V.; et al. Middle Miocene Closure of the Central American Seaway. *Science* **2015**, *348*, 226–229. [CrossRef]
107. O'Dea, A.; Lessios, H.A.; Coates, A.G.; Eytan, R.I.; Restrepo-Moreno, S.A.; Cione, A.L.; Collins, L.S.; De Queiroz, A.; Farris, D.W.; Norris, R.D.; et al. Formation of the Isthmus of Panama. *Sci. Adv.* **2016**, *2*, e1600883. [CrossRef] [PubMed]
108. Jaramillo, C. Evolution of the Isthmus of Panama: Biological, Paleoceanographic and Paleoclimatological Implications. In *Mountains, Climate and Biodiversity*; Hoorn, C., Perrigo, A., Antonelli, A., Eds.; John Wiley & Sons Ltd.: Hoboken, NJ, USA, 2018; pp. 323–338.
109. Mora, A.; Villagómez, D.; Parra, M.; Caballero, V.M.; Spikings, R.; Horton, B.K.; Mora-Bohórquez, J.A.; Ketcham, R.A.; Arias-Martínez, J.P. Chpt 4: Late Cretaceous to Cenozoic uplift of the northern Andes: Paleogeographic implications. In *The Geology of Colombia, Volume 3 Paleogene—Neogene*; Gómez, J., Mateus–Zabala, D., Eds.; Servicio Geológico Colombiano, Publicaciones Geológicas Especiales: Bogotá, Colombia, 2020; Volume 37, pp. 89–121. [CrossRef]
110. Mothé, D.; Jaramillo, C.; Krigsfeld Shuster, G.; Oikawa, N.; Escobar-Florez, S. Ain't No Mountain High Enough? New Records of *Notiomastodon platensis* (Mammalia, Proboscidea) from Colombia and the Quaternary Dry Corridor of the *Cauca* Valley. *Hist. Biol.* **2024**, *36*, 241–252. [CrossRef]
111. Nei, M.; Maruyama, T.; Chakraborty, R. The Bottleneck Effect and Genetic Variability in Populations. *Evolution* **1975**, *29*, 1–10. [CrossRef] [PubMed]
112. Whyte, I.; Van Aarde, R.; Pimm, S.L. Managing the Elephants of Kruger National Park. *Anim. Conserv.* **1998**, *1*, 77–83. [CrossRef]
113. de Silva, S. On Predicting Elephant Population Dynamics. *Gajah* **2010**, *33*, 12–16.
114. Turkalo, A.K.; Wrege, P.H.; Wittemyer, G. Slow Intrinsic Growth Rate in Forest Elephants Indicates Recovery from Poaching Will Require Decades. *J. Appl. Ecol.* **2017**, *54*, 153–159. [CrossRef]
115. Baker, A.J.; Moeed, A. Rapid Genetic Differentiation and Founder Effect in Colonizing Populations of Common Mynas (*Acridotheres tristis*). *Evolution* **1987**, *41*, 525–538. [CrossRef]
116. BirdLife Data Zone 2025 Common Myna *Acridotheres tristis* Species Fact Sheet. Available online: https://datazone.birdlife.org/species/factsheet/common-myna-acridotheres-tristis (accessed on 18 December 2025).
117. Wittemyer, G.; Daballen, D.; Douglas-Hamilton, I. Comparative Demography of an At-Risk African Elephant Population. *PLoS ONE* **2013**, *8*, e53726. [CrossRef]
118. Palkopoulou, E.; Dalén, L.; Lister, A.M.; Vartanyan, S.; Sablin, M.; Sher, A.; Edmark, V.N.; Brandström, M.D.; Germonpré, M.; Barnes, I.; et al. Holarctic Genetic Structure and Range Dynamics in the Woolly Mammoth. *Proc. R. Soc. B Biol. Sci.* **2013**, *280*, 20131910. [CrossRef]
119. Bacon, C.D.; Silvestro, D.; Jaramillo, C.; Smith, B.T.; Chakrabarty, P.; Antonelli, A. Biological Evidence Supports an Early and Complex Emergence of the Isthmus of Panama. *Proc. Natl. Acad. Sci. USA* **2015**, *112*, 6110–6115. [CrossRef] [PubMed]
120. Casamiquela, R.M.; Shoshani, J.; Dillehay, T.D. South American Proboscideans: General Introduction and Reflections on Pleistocene Extinctions. In *The Proboscidea*; Shoshani, J., Tassy, P., Eds.; Oxford University Press: Oxford, UK, 1996; pp. 316–320.
121. Sanchez, G.; Holliday, V.T.; Gaines, E.P.; Arroyo-Cabrales, J.; Martínez-Tagüeña, N.; Kowler, A.; Lange, T.; Hodgins, G.W.L.; Mentzer, S.M.; Sanchez-Morales, I. Human (Clovis)–Gomphothere (*Cuvieronius* sp.) Association ~13,390 Calibrated yBP in Sonora, Mexico. *Proc. Natl. Acad. Sci. USA* **2014**, *111*, 10972–10977. [CrossRef] [PubMed]

122. Reguero, M.A.; Candela, A.M.; Alonso, R.N. Biochronology and Biostratigraphy of the Uquía Formation (Pliocene–Early Pleistocene, NW Argentina) and Its Significance in the Great American Biotic Interchange. *J. S. Am. Earth Sci.* **2007**, *23*, 1–16. [CrossRef]
123. Woodburne, M.O.; Cione, A.L.; Tonni, E.P. Central American Provincialism and the Great American Biotic Interchange. In *Advances in Late Tertiary Vertebrate Paleontology in Mexico and the Great American Biotic Interchange*; Carranza-Castaneda, Ó., Lindsay, E.H., Eds.; Universidad Nacional Autónoma de México, Instituto de Geología and Centro de Geociencias: Mexico City, Mexico, 2006; Publicación Especial; pp. 73–101. Available online: https://www.researchgate.net/publication/228461083_Central_American_provincialism_and_the_Great_America_Biotic_Interchange (accessed on 18 December 2025).
124. Hoppe, K.A. The Biogeochemistry and Paleoecology of Late Pleistocene Proboscideans from the Southern United States. Ph.D. Thesis, Princeton University, Princeton, NJ, USA, 1999. DAI-B 60/11, Dissertation Abstracts International, Dissertation/thesis number 9948639.
125. Bonhof, W.J.; Pryor, A.J.E. Proboscideans on Parade: A Review of the Migratory Behaviour of Elephants, Mammoths, and Mastodons. *Quat. Sci. Rev.* **2022**, *277*, 107304. [CrossRef]
126. Miller, J.H.; Fisher, D.C.; Crowley, B.E.; Secord, R.; Konomi, B.A. Male Mastodon Landscape Use Changed with Maturation (Late Pleistocene, North America). *Proc. Natl. Acad. Sci. USA* **2022**, *119*, e2118329119. [CrossRef]
127. Kowalik, N.; Anczkiewicz, R.; Müller, W.; Spötl, C.; Bondioli, L.; Nava, A.; Wojtal, P.; Wilczyński, J.; Koziarska, M.; Matyszczak, M. Revealing Seasonal Woolly Mammoth Migration with Spatially-Resolved Trace Element, Sr and O Isotopic Records of Molar Enamel. *Quat. Sci. Rev.* **2023**, *306*, 108036. [CrossRef]
128. McCloskey, J. A Multi-Isotope Investigation of Mammoth Diet, Habitat, and Movement Patterns in the Central Great Plains, USA. Ph.D. Thesis, University of Nebraska-Lincoln, Lincoln, NE, USA, 2025. Department of Earth and Atmospheric Sciences: Dissertations, Theses, and Student Research. 174. Available online: https://digitalcommons.unl.edu/geoscidiss/174 (accessed on 18 December 2025).
129. Van Der Valk, T.; Pečnerová, P.; Díez-del-Molino, D.; Bergström, A.; Oppenheimer, J.; Hartmann, S.; Xenikoudakis, G.; Thomas, J.A.; Dehasque, M.; Sağlıcan, E.; et al. Million-Year-Old DNA Sheds Light on the Genomic History of Mammoths. *Nature* **2021**, *591*, 265–269. [CrossRef]
130. Debruyne, R.; Chu, G.; King, C.E.; Bos, K.; Kuch, M.; Schwarz, C.; Szpak, P.; Gröcke, D.R.; Matheus, P.; Zazula, G.; et al. Out of America: Ancient DNA Evidence for a New World Origin of Late Quaternary Woolly Mammoths. *Curr. Biol.* **2008**, *18*, 1320–1326. [CrossRef]
131. Arrieta-Donato, E.; Tavares-Guzmán, Á.; Bravo-Lopez, M.; Villa-Islas, V.; Castillo-Carbajal, A.; Li, W.; Garfias-Morales, E.; Padilla-Bustos, R.; Sandoval-Velasco, M.; Córdoba-Barradas, L.; et al. Columbian Mammoth Mitogenomes from Mexico Uncover the Species' Complex Evolutionary History. *Science* **2025**, *390*, 47–52. [CrossRef]
132. Lister, A.M.; Sher, A.V.; Van Essen, H.; Wei, G. The Pattern and Process of Mammoth Evolution in Eurasia. *Quat. Int.* **2005**, *126–128*, 49–64. [CrossRef]
133. Karpinski, E.; Hackenberger, D.; Zazula, G.; Widga, C.; Duggan, A.T.; Golding, G.B.; Kuch, M.; Klunk, J.; Jass, C.N.; Groves, P.; et al. American Mastodon Mitochondrial Genomes Suggest Multiple Dispersal Events in Response to Pleistocene Climate Oscillations. *Nat. Commun.* **2020**, *11*, 4048. [CrossRef] [PubMed]
134. Nyakaana, S.; Arctander, P. Population Genetic Structure of the African Elephant in Uganda Based on Variation at Mitochondrial and Nuclear Loci: Evidence for Male-biased Gene Flow. *Mol. Ecol.* **1999**, *8*, 1105–1115. [CrossRef] [PubMed]
135. Wooller, M.J.; Bataille, C.; Druckenmiller, P.; Erickson, G.M.; Groves, P.; Haubenstock, N.; Howe, T.; Irrgeher, J.; Mann, D.; Moon, K.; et al. Lifetime Mobility of an Arctic Woolly Mammoth. *Science* **2021**, *373*, 806–808. [CrossRef]
136. de Flamingh, A.; Sole, C.L.; van Aarde, R.J. Genetic Evidence for Spatial Structuring in a Continuous African Elephant (*Loxodonta africana*) Population. *Conserv. Genet.* **2015**, *16*, 613–623. [CrossRef]
137. Enk, J.; Devault, A.; Widga, C.; Saunders, J.; Szpak, P.; Southon, J.; Rouillard, J.-M.; Shapiro, B.; Golding, G.B.; Zazula, G.; et al. *Mammuthus* Population Dynamics in Late Pleistocene North America: Divergence, Phylogeography, and Introgression. *Front. Ecol. Evol.* **2016**, *4*, 42. [CrossRef]
138. Avise, J.C.; Robinson, T.J. Hemiplasy: A New Term in the Lexicon of Phylogenetics. *Syst. Biol.* **2008**, *57*, 503–507. [CrossRef]
139. Moore, W.S. Inferring Phylogenies from mtDNA Variation: Mitochondrial-Gene Trees Versus Nuclear-Gene Trees. *Evolution* **1995**, *49*, 718. [CrossRef]
140. Smith, B.T.; Klicka, J. Examining the Role of Effective Population Size on Mitochondrial and Multilocus Divergence Time Discordance in a Songbird. *PLoS ONE* **2013**, *8*, e55161. [CrossRef]
141. Coltorti, M.; Abbazzi, L.; Ferretti, M.P.; Iacumin, P.; Rios, F.P.; Pellegrini, M.; Pieruccini, P.; Rustioni, M.; Tito, G.; Rook, L. Last Glacial Mammals in South America: A New Scenario from the Tarija Basin (Bolivia). *Naturwissenschaften* **2007**, *94*, 288–299. [CrossRef]

142. Borrero, L.A. The Elusive Evidence: The Archeological Record of the South American Extinct Megafauna. In *American Megafaunal Extinctions at the End of the Pleistocene*; Haynes, G., Ed.; Vertebrate Paleobiology and Paleoanthropology; Springer Netherlands: Dordrecht, The Netherlands, 2009; pp. 145–168. Available online: https://linkinghub.elsevier.com/retrieve/pii/S0960982208009706 (accessed on 18 December 2025).
143. Song, S.; Liu, L.; Edwards, S.V.; Wu, S. Resolving Conflict in Eutherian Mammal Phylogeny Using Phylogenomics and the Multispecies Coalescent Model. *Proc. Natl. Acad. Sci. USA* **2012**, *109*, 14942–14947. [CrossRef] [PubMed]
144. Mehta, R.S.; Rosenberg, N.A. The Probability of Reciprocal Monophyly of Gene Lineages in Three and Four Species. *Theor. Popul. Biol.* **2018**, *129*, 133–147. [CrossRef] [PubMed]
145. Caragiulo, A.; Dias-Freedman, I.; Clark, J.A.; Rabinowitz, S.; Amato, G. Mitochondrial DNA Sequence Variation and Phylogeography of Neotropic Pumas (*Puma concolor*). *Mitochondrial DNA* **2014**, *25*, 304–312. [CrossRef]
146. Culver, M.; Johnson, W.; Pecon-Slattery, J.; O'Brien, S. Genomic Ancestry of the American Puma (*Puma concolor*). *J. Hered.* **2000**, *91*, 186–197. [CrossRef]
147. Rohland, N.; Reich, D.; Mallick, S.; Meyer, M.; Green, R.E.; Georgiadis, N.J.; Roca, A.L.; Hofreiter, M. Genomic DNA Sequences from Mastodon and Woolly Mammoth Reveal Deep Speciation of Forest and Savanna Elephants. *PLoS Biol.* **2010**, *8*, e1000564. [CrossRef] [PubMed]

Disclaimer/Publisher's Note: The statements, opinions and data contained in all publications are solely those of the individual author(s) and contributor(s) and not of MDPI and/or the editor(s). MDPI and/or the editor(s) disclaim responsibility for any injury to people or property resulting from any ideas, methods, instructions or products referred to in the content.